EFFECT OF PUMPING RATES ON LONG-TERM AQUIFER STORAGE AND RECOVERY WELL PERFORMANCE FOR CONSERVATIVE AND REACTIVE TRANSPORT SCENARIOS

A Thesis

by

PATRICK CARPENTER

Submitted to the Office of Graduate and Professional Studies of
Texas A&M University
in partial fulfillment of the requirements for the degree of

MASTER OF SCIENCE

Chair of Committee,	Gretchen Miller
Committee Members,	Zhuping Sheng
	Hongbin Zhan
Head of Department,	Ronald Kaiser

August 2020

Major Subject: Water Management and Hydrological Science

Copyright 2020 Patrick Carpenter

ABSTRACT

Recovery of injected water is one of the most important aspects of an aquifer storage and recovery (ASR) system and is determined by hydrogeologic, operational, and chemical factors. A common series of reactions resulting in deterioration of water quality is the release of arsenic via pyrite oxidation. Previous work suggests system performance can be affected by altering pumping rates while maintaining a constant volume; this is verified in the conservative transport portion of the study. In addition, this study explores the effect of altered pumping rates on arsenic release via pyrite oxidation.

A single ASR well in a confined homogenous aquifer was simulated for a range of hydraulic gradients and storage durations for ten cycles to quantify the effect of pumping rates on system performance for conservative transport using numerical modeling. Reactive transport capabilities were added to a subset of these models to analyze the effects of altering pumping rates on arsenic release via pyrite dissolution.

The simulation results showed that performance improved with higher injection and extraction rates for all combinations of hydraulic gradient and storage period considered, although the magnitude of improvement over the baseline scenario was greater for higher hydraulic gradients and longer storage periods. Extraction rates were more influential on system performance than injection rates, with the best and worst performance experienced during the fast and slow extraction scenarios, respectively.

Longer storage periods result in more total arsenic released and higher average recovered arsenic concentrations. Injection and extraction rates have their own impact on arsenic release via pyrite dissolution. Injection rates control the spatial extent of dissolved oxygen around the

well, with higher rates resulting in a larger extent. Extraction rates affected the amount of arsenic released by controlling the residence time of dissolved oxygen. Higher extraction rates resulted in less residence time of dissolved oxygen and less arsenic released overall. Both higher extraction and injection rates resulted in lower recovered arsenic concentrations; however, regardless of pumping rate, recovered arsenic concentrations were below the EPA's MCL by the second cycle. Results also highlight the need to manage sorbed arsenic and the injected water plume carefully in aquifers containing arsenic-bearing pyrite lest arsenic migrates beyond the well's capture zone and affects downgradient users.

ACKNOWLEDGEMENTS

I would like to thank my advisor, Dr. Gretchen Miller, for guidance over the course of this project. I would also like to thank my committee members, Dr. Hongbin Zhan and Dr. Zhuping Sheng, for their input and suggestions.

Thanks to my friends and family, especially my parents, for their support in this seemingly never-ending time.

CONTRIBUTORS AND FUNDING SOURCES

This work was supervised by a thesis committee consisting of Dr. Gretchen Miller [advisor] of the Department of Civil Engineering at Texas A&M University, Dr. Hongbin Zhan of the Department of Geology and Geophysics at Texas A&M University, and Dr. Zhuping Sheng of the Texas A&M AgriLife Research and Extension Center at El Paso and the Department of Biological and Agricultural Engineering at Texas A&M University. All work for the thesis was completed independently by the student.

Graduate study was supported in part by the WMHS program at Texas A&M University.

NOMENCLATURE

ASR	Aquifer Storage and Recovery
DO	Dissolved Oxygen
EPA	Environmental Protection Agency
HFO	Hydrous Ferric Oxide
RE	Recovery Efficiency
REN	Recovery Effectiveness

TABLE OF CONTENTS

Page

LIST OF FIGURES

Page

LIST OF TABLES

Page

1. INTRODUCTION

1.1 ASR Overview

Aquifer storage and recovery (ASR) is a water management technique in which water is injected into an aquifer during times of excess and recovered when necessary, with both injection and extraction occurring in the same well (Dillon et al., 2009; Pyne, 2005). An ASR system can consist of one well (Antoniou et al., 2012; Zuurbier et al., 2016) or multiple wells (Forghani et al., 2017; Sheng, 2005; Webb, 2015). In addition to its primary purpose of balancing supply and demand, ASR can also increase groundwater levels, provide a barrier against saltwater intrusion, and bolster environmental streamflows (Pyne, 2005; Pyne, 2015). Compared to surface water reservoirs, ASR systems have essentially no evaporative loss, minimal environmental impacts and land use demands, and lower costs (Dillon et al., 2009; Khan et al., 2008; Maliva et al., 2006). Evaporation in surface reservoirs is substantial in semi-arid to arid environments and is expected to increase in the future due to warmer climates (Helfer et al. 2012; Wang et al., 2018; Wurbs et al., 2015; Zhang et al., 2017); due to this, ASR may be a viable drought-resistant alternative to surface reservoirs for water management.

Prior to injection, source water is generally treated to drinking water standards to prevent the deterioration of ambient groundwater quality, the onset of undesired chemical reactions, and clogging of the well screen (Pyne, 2005; Drewes, 2009). ASR can be performed in both freshwater and saline aquifers, and has proven effective with different types of source water including: reclaimed wastewater (Dillon et al., 2009; Missimer et al., 2012; Sheng, 2005), treated surface water (Maliva et al., 2006), and groundwater from another aquifer (Webb, 2015). Urban stormwater may be used for ASR, although its high dissolved organic carbon (DOC) content may negatively impact groundwater quality due to its effect on subsurface reactions (Antoniou et

al. 2015; Vanderzalm et al. 2010). Although ASR can be performed in both confined and unconfined aquifers, higher groundwater velocities, closer proximity to the surface and contamination sources, and overlying land use make confined aquifers better choices for an ASR system (Pyne, 2005). ASR is viable in different geologic media and has been implemented globally.

ASR system performance is generally determined by the amount of recovered water of usable quality, which can be calculated in a few ways. In saline aquifers where mixing between source and ambient water is allowed, recovery efficiency (*RE*) is the standard metric (Bakker, 2010; Forghani and Peralta, 2018). Recovery efficiency is the ratio of the volume of recovered water of a certain quality to the volume of injected water (Eq. 1). Recovery efficiency is calculated using some concentration limit, usually the EPA's secondary standard of 500 mg/L for total dissolved solids (TDS), to signal the end of extraction.

$$RE = \frac{V_{rec}}{V_{inj}} \quad (1)$$

where V_{rec} is the volume of recovered water at acceptable quality [L^3], and V_{inj} is the volume of injected water [L^3]. Recovery efficiency is useful in situations where mixing between the ambient and injected water is permissible, and the waters have significantly different chemistries or salinity levels.

1.2 Factors Affecting ASR performance

1.2.1 Hydrogeologic Parameters

Hydrogeologic parameters that affect ASR performance include, but are not limited to: hydraulic conductivity, hydraulic gradient, longitudinal dispersivity, aquifer heterogeneity, and aquifer thickness (Bakker, 2010; Forghani and Peralta, 2017; Guo et al. 2014; Lowry & Anderson, 2006; Lu et al., 2011; Smith et al. 2017; Ward et al., 2009). Hydraulic conductivity

should ideally be in a "sweet spot" for ASR operations; low or high values of hydraulic conductivity can result in reduced recovery efficiency (Lowry & Anderson 2006; Maliva & Missimer, 2010; Smith et al. 2017). Performing ASR in low hydraulic conductivity zones can result in reduced injection rates and large head variations at the well (Forghani et al., 2018; Ward et al., 2009). In aquifers with high hydraulic conductivity, lateral migration of injected water past the well capture zone becomes a primary concern (Maliva & Missimer, 2010; Ward et al., 2009).

Small regional hydraulic gradients are desired in ASR storage zones, as high hydraulic gradients can affect an ASR system during injection, storage, and recovery. If gradients are high, neither the injected water plume nor the well's capture zone can be assumed circular (Ceric and Haitjema, 2005; Ward et al. 2009), and during storage, some or all of the injected water will migrate away from the well and become unrecoverable, lowering the recovery efficiency (Pavelic et al. 2004; Lowry & Anderson 2006; Ward et al. 2009; Smith et al. 2017). Increasing hydraulic gradient was found to decrease recovery efficiencies in three different hydrogeologic settings, though the effect of hydraulic gradient was much more drastic in the settings with high hydraulic conductivity (Lowry & Anderson 2006). This agrees with Forghani and Peralta (2017), who found that *REN* was most strongly correlated with hydraulic gradient and hydraulic conductivity.

The length of the storage period must also be considered in conjunction with the hydraulic gradient, as long storage periods can magnify the effects of a small hydraulic gradient (Ward et al. 2009; Smith et al. 2017). The combined effects of storage time and hydraulic gradient are described by the technical viability ratio (R_{TV}) of Ward et al. (2009) (Eq. 4), where lower values of R_{TV} are more desirable.

$$\mathbf{R_{TV}} = \frac{\mathbf{K_{x,ave} I t_{storage}}}{\boldsymbol{\varepsilon} \mathbf{x_{i,upstream}}} \quad (2)$$

where $K_{x,ave}$ is the average horizontal hydraulic conductivity [L/T], I is hydraulic gradient [-], $t_{storage}$ is the storage duration [T], ε is the porosity [-], and $x_{i,upstream}$ is the upgradient location of the injected and ambient water interface [L]. Details on how to calculate $x_{i,upstream}$ using $\bar{t}$ (discussed later, Eq. 8), aquifer thickness, pumping rate, hydraulic conductivity, and hydraulic gradient can be found in Ward et al. (2009).

Dispersive mixing of injected and native waters during injection and storage will decrease the recovery efficiency of an ASR system (Lowry & Anderson, 2006; Ward et al., 2009). Longitudinal dispersivity describes the spreading of a plume in the direction of groundwater flow; it is a measure of the aquifer's heterogeneity and, due to lack of field data is generally calibrated from observed data (Schulze-Makuch, 2005; Forghani and Peralta, 2017). With more accurate characterization of an aquifer's heterogeneity, and grid sizes small enough to represent those heterogeneities, the smaller the calibrated values of longitudinal dispersivity will be (Davis, 1986; Konikow, 2011). Longitudinal dispersivity is also a scale-dependent property, following the empirical power law of Schulze-Makuch (2005) (Eq. 5).

$$\boldsymbol{\alpha} = \mathbf{c}(\mathbf{L})^{\mathbf{m}} \quad (3)$$

where α is the longitudinal dispersivity [L], c is the aquifer type parameter [L^{-1}], and m is the scaling exponent [-]. Values for c and m and more information on their derivation can be found in Schulze-Makuch (2005).

Compared to ASR systems in aquifers with a homogeneous distribution of hydraulic conductivity, ASR systems in heterogeneous aquifers in the storage zone can result in preferential flow paths that will decrease the recovery efficiency (Guo et al. 2014). Increasing

heterogeneity results in more mixing and decreased recovery efficiency. Increasing aquifer thickness has a negative impact on recovery efficiency (Ward et al., 2009; Bakker, 2010; Forghani and Peralta, 2018).

1.2.2 Operational Parameters

Operational parameters that affect ASR performance include pumping rate, pumping duration, and storage time (Ward et al., 2009; Bakker, 2010; Lu et al., 2011; Forghani and Peralta, 2018; Fatkhutdinov & Stefan, 2019). Ward et al. (2009) developed four dimensionless numbers to describe the effects of lateral flow, density-driven flow, and dispersivity on the initial cycle of an ASR operation in brackish aquifers; if the sum of the four numbers, R_{ASR}, was less than 0.1, then the operation was likely to result in high mixing fractions after the first cycle. Each of these dimensionless numbers were calculated using the location of the interface between injected and ambient water, $x_{i,upstream}$, which is dependent on the dimensionless time parameter, $\bar{t}$ (Eq. 6). These dimensionless numbers were found to be consistent with field data from six sites in Florida (Ward et al., 2009). In general, higher pumping rates and lower pumping durations and storage times resulted in higher mixing fractions at the end of recovery; however, these effects were only studied for the initial cycle of ASR.

$$\bar{t} = \frac{2\pi t_{injection} B}{\varepsilon Q} (K_{x,ave} I)^2 \quad (4)$$

where $t_{injection}$ is the length of the injection period [T], B is aquifer thickness [L], Q is the pumping rate [L^3/T], $K_{x,ave}$ is the average horizontal hydraulic conductivity [L^2/T], and I is the hydraulic gradient [-].

Bakker (2010) found that recovery efficiency in a saline aquifer was determined by one dimensionless parameter, *D* (Eq. 7), and the relative lengths of the injection, storage, and

recovery phases. Recovery efficiency is maximized when *D* is large and storage time is small. Both Ward's R_{ASR} and Bakker's *D* were compared to field data of nine existing ASR systems in the Netherlands and were both found to be reasonable predictors of ASR performance (Zuurbier et al., 2013). A detailed comparison of Ward's R_{ASR} and Bakker's *D* can be found in Zuurbier et al. (2013).

$$\mathrm{D} = \frac{\mathrm{Q}}{\mathrm{KvH}^2} \tag{5}$$

where *Q* is the pumping rate, *K* is the horizontal hydraulic conductivity, *v* is the dimensionless density difference (Eq. 8), and *H* is the aquifer thickness.

Lu et al. (2011) developed five dimensionless operational parameters based on first order mass transfer and studied their effects on the recovery efficiency of a simulated ASR operation; they found that recovery efficiency generally improves over multiple ASR cycles and that ASR scenarios with zero recovery efficiency on the first cycle could, over multiple cycles, be transformed into an ASR operation with positive recovery efficiency. For a single ASR cycle, recovery efficiencies were found to increase with increasing pumping rate and injection time. However, Lu et al. (2011) did not consider the effects of regional flow, which Ward et al. (2009) showed to have an impact on mixing fractions of the ASR operation, nor did they consider the effects of variable pumping rates over multiple cycles of injection

Fatkhutdinov & Stefan (2019) used a multi-objective hybrid global/local optimization algorithm to determine optimal pumping rates over 10 cycles of ASR as a function of total dissolved solids concentrations at the well. TDS concentration at the well were found to increase with decreasing average pumping rates (both injection and extraction). However, Fatkhutdinov

& Stefan (2019) did not consider the effects of variable injection rates, hydrogeologic parameters, or storage time on the optimal abstraction rates.

1.2.3 Oxidation of Pyrite

Pyrite is a sulfide mineral with the chemical formula FeS_2 and is commonly found in sedimentary rocks (Klein & Dutrow, 2007). Despite the near 2:1 ratio of sulfur to iron, pyrite can include a wide array of elements as substitutions for both iron and sulfur, including arsenic which substitutes for sulfur(Abraitis et al., 2003). Arsenic can comprise up to 10% of the weight of pyrite sample, and its inclusion can make the mineral metastable and accelerate its dissolution under oxidizing conditions (Abraitis et al. 2003; Blanchard et al. 2006; Neil et al., 2012). The distinction is made here between arsenian pyrite ($FeAs_xS_{2-x}$) and arsenopyrite (FeAsS), which is more stable than arsenian pyrite and dissolves under acidic or oxidizing conditions (Neil et al., 2012).

Chemical differences between source water and ambient water can result in subsurface reactions, mobilization of trace elements, and deterioration of water quality. Because source waters are typically equilibrated with the atmosphere, they usually contain higher dissolved oxygen (DO) concentrations than found in native groundwater (Antoniou et al., 2015; Neil et al., 2012; Pyne, 2005). Injection of water containing elevated DO shifts the redox conditions near the well from reducing to oxidizing, which results in the dissolution of pyrite and mobilization of arsenic (Jones and Pichler 2007; Lazareva et al. 2015; Neil et al. 2018; Wallis et al. 2010; Wallis et al. 2011). The reactions following injection of water high in DO are summarized in Table 1. Arsenic is released from pyrite as arsenite which can be oxidized to arsenate, with adequate DO (Antoniou et al., 2015). Arsenate is less mobile than arsenite because it preferentially sorbs on hydrous ferric oxides, or HFO (Antoniou et al., 2017; Wallis et al., 2011).

Table 1. Core reactions for release and sorption of arsenic in aquifers containing As-pyrite.

Reaction	Description
$FeAs_xS_{2-x}(s) + \frac{3}{2}H_2O + \frac{11}{4}O_2(aq) = (2-X)SO_4^{2-} + Fe^{2+} + XH_3AsO_3$ (aq)	Dissolution of arsenic-bearing pyrite
$4Fe^{2+} + O_2 + 10H_2O = 4Fe(OH)_3(s) + 8H^+$	Precipitation of ferrihydrite
$Fe(OH)_3\_wOH + AsO_4^{-3} + 3H^+ = Fe(OH)_3\_wH_2AsO_4 + H_2O$ $Fe(OH)_3\_wOH + AsO_4^{-3} + 2H^+ = Fe(OH)_3\_wHAsO_4^- + H_2O$ $Fe(OH)_3\_wOH + AsO_4^{-3} = Fe(OH)_3\_wOHAsO_4^{-3}$ $Fe(OH)_3\_wOH + H_3AsO_3 = Fe(OH)_3\_wH_2AsO_3 + H_2O$	Sorption of arsenite and arsenate on ferrihydrite

Fe(II) is also released into solution following the dissolution of pyrite. If DO is present, Fe(II) is further oxidized to Fe(III) and precipitates as ferrihydrite, or hydrous ferric oxide (HFO) (Antoniou et al., 2017; Neil et al., 2012). Sorption of arsenic onto HFO's is the main attenuation process of mobilized arsenic and can limit its lateral migration during the injection and storage phases (Antoniou et al., 2017; Mirecki et al., 2013; Neil et al., 2012; Wallis et al., 2011). During recovery, however, as redox conditions near the well shift back to reducing, HFO's dissolve and release sorbed arsenic to solution, which can exceed the EPA's MCL of 10 μg/L in arsenic (Antoniou et al., 2015; Neil et al., 2012; Wallis et al., 2011). Not all HFO dissolves at the end of each cycle which leads to a gradual increase in HFO concentrations and sorbed arsenic mass. Gradual increase in HFO concentrations could become a clogging concern, although the magnitude of this impact has not been explored (Jeong et al., 2018; Martin, 2013).

1.3 Knowledge Gap & Objectives of Study

While certain aquifer characteristics, such as low gradients and hydraulic conductivity, are preferable in an ASR system, it may not be feasible to implement an ASR operation in these locations due to other considerations, such as: proximity to source water, proximity to the population to be served, incompatible source water and ambient water, depth to aquifer, and nearby well density, among other reasons (Amineh et al., 2017; Smith et al., 2017). Once a site is chosen for an ASR system, there are fixed aquifer parameters, and modification of operational parameters becomes the only way to affect the ASR system's performance. Considering the factors mentioned above, understanding the expected performance and potential improvement of an ASR system under different hydrogeologic conditions would be beneficial.

Previous studies have considered the effect of altering the injection rate on system performance but did so by holding the length of the injection period constant, effectively only altering the volume of injected water (Forghani & Peralta, 2018; Ward et al., 2009). Increasing the volume of injected water has previously been shown to positively impact the performance of an ASR system (Lowry & Anderson, 2006), but no known studies have shown the effect of injecting or extracting a given volume of water in a certain way, i.e. via fast or slow injection/extraction. This constant-volume approach is logical because not all water utilities can simply increase the volume of water available for injection. The extraction period is treated similarly in previous studies, resulting in variable extracted volumes, sometimes exceeding the volume of water injected (Fatkhutdinov & Stefan, 2019; Forghani & Peralta, 2018; Ward et al., 2009). This study maintains a constant injected and extracted volume by simultaneously changing the length of the pumping periods and the pumping rates.

Altering the pumping rates of an ASR system can affect the mixing fraction at the well (Ward et al., 2009), which should have an effect on subsurface reactions due their different chemistries. Recent studies have found that increased pumping rates in supply wells results in lower recovered arsenic concentrations; however, the aquifers in these studies have seasonal variations in water chemistry, have layers with different chemistries, or both (Bexfield & Jurgens, 2014; Degnan et al., 2020) Studies to date have not considered the effect of variable injection and extraction rates on the oxidation of pyrite and behavior of arsenic in the context of an ASR system.

The objectives of this study are to: analyze the effects of altering pumping rates on long-term ASR performance for a given volume of water over a range of hydrogeologic conditions, test under which hydrogeologic environments and storage durations ASR performance can be expected to improve, compare the impact of injection vs. storage time on ASR performance, and to determine the impact of altering the injection and extraction rates on arsenic behavior in an aquifer containing arsenic-bearing pyrite. The proposed work will be of benefit to those who wish to understand the long-term improvement of an ASR operation and the effect of variable pumping rates on pyrite oxidation.

2. METHODS

2.1 Introduction

To address the objectives listed above, a hypothetical ASR well in a confined aquifer was simulated. Flow, conservative transport, and reactive transport models were run in Python using the FloPy package, which allows the user to create, run, and post-process MODFLOW, MT3D, SEAWAT, and related software using Python scripts (Bakker et al., 2016). FloPy provides all the packages and versatility of Python, allows for easy modification of model parameters and discretization, and can result in faster run times for simulations than when using a GUI (Bakker et al. 2016). Executables used to calculate flow and conservative transport in Python are MODFLOW-2005 and MT3D-USGS, respectively (Bedekar et al., 2016; Harbaugh, 2005). While the PHT3D-PHREEQC interface (PHC) package for MT3DMS is supported in FloPy, the script which creates the file required some modifications to create a properly formatted interface file (Appendix A). The executable used for reactive transport was PHT3D v2.10.

2.2 Flow Model Setup

For the purposes of this study, a single fully-screened ASR well was simulated in a hypothetical confined aquifer using reasonable values of hydraulic conductivity, porosity, and specific storage (Heath, 1983). Model input parameters are given in Table 2. The model extent is 1,500 m square and 100 m thick. Constant head boundaries were set on both sides of the model domain to set a lateral flow. Horizontal and vertical discretization is 5 m in the all directions to satisfy the grid Peclet number constraint; the grid Peclet number is the ratio of the grid cell size to longitudinal dispersivity and should be less than four to minimize numerical dispersion and artificial oscillation (Ward et al., 2009; Zheng and Bennett, 2002). The aquifer is

assumed to be homogeneous and is simulated over a range of specific discharge rates, from 0.001 to 0.05 m/d.

Table 2. Conservative transport model input parameters

Property	Value
Aquifer thickness (m)	100
Horizontal discretization (m)	5
Model extent (m)	1,500 x 1,500
Hydraulic Conductivity (m/d)	10
Vertical Hydraulic Conductivity (m/d)	1
Hydraulic gradient (-)	0.0001, 0.001, 0.0025, 0.005
Specific storage	0.0004
Injected volume (m^3)	315,000
Pumping duration (d)	40, 90, 140
Pumping rate (m^3/d)	2250, 3500, 7875
Longitudinal dispersivity (m)	5
Injected water concentration (mg/L)	0
Ambient water concentration (mg/L)	1,000

The ASR well was simulated under a range of pumping and storage scenarios and repeated for ten cycles to show long-term effects. Three storage durations were considered: zero days, six months (baseline), and one year. These storage durations were chosen to compare the best possible ASR performance (zero-day storage) with that of an ASR system with a typical storage duration. The injected and extracted volume of each cycle was held constant at 315,000 m^3, varying only the pumping rates and durations. Three pumping rates and durations were considered: ± 7,875 m^3/d for 40 days (fast injection/extraction), ± 3,500 m^3/d for 90 days (baseline), and ± 2,250 m^3/d for 140 days (slow injection/extraction). When altering the injection rate, the extraction rate was held constant at 3,500 m^3/d, and vice versa. This was done to show the relative impact of injection rates vs. extraction rates.

2.3 Conservative Transport Model Setup

Conservative transport models were run to assess the performance of each combination of ASR operational parameters and hydrogeologic conditions. Because transport is calculated based on the simulated flow field, there is presently no way to simulate termination of pumping based on a concentration limit. Due to this limitation, the entire injected volume is recovered in each recovery phase. Well performance was calculated using two indicators: mixing fraction at the end of extraction and cumulative Recovery Effectiveness. Mixing fraction, *f*, is the proportion of injected water in a sample of recovered water at a given time (Harpaz and Bear, 1964; Ward et al., 2009).

$$\mathbf{f} = \frac{\mathbf{C_{amb} - C_{mix}}}{\mathbf{C_{amb} - C_{inj}}} \quad (6)$$

where C_{amb} is the tracer concentration in the ambient water, C_{mix} is the tracer concentration in the sample, and C_{inj} is the tracer concentration in the injected water. The mixing fraction at the end of extraction gives an indication of the degree of mixing occurring between the injected and native water, with higher values of *f* indicating less mixing.

REN is the proportion of injected water recovered by the well, and is given by:

$$\mathrm{REN} = \frac{\mathrm{V_{E_{inj}}}}{\mathrm{V_{inj}}} \quad (7)$$

where $V_{E_{inj}}$ is the volume of injected water within the volume of extracted water [L^3]. $V_{E_{inj}}$ is calculated following Pyne (2005) (Eq. 4).

$$\mathbf{V_{E_{inj}}} = \int_{\mathbf{t=start\ of\ extraction}}^{\mathbf{t=end\ of\ extraction}} \mathbf{f} \cdot \mathbf{Q_{ext}}\, \mathbf{dt} \quad (8)$$

Where Q_{ext} is the extraction rate [L^3/T]. The cumulative *REN* (REN_{cum}) for multiple cycles can be calculated by summing Eq. 3 for the total number of cycles, *m* (Eq. 5).

$$REN_{cum} = \sum_{t=1}^{m} \frac{V_{E_{inj}}}{V_{inj}} \quad (9)$$

The ambient and injected water were assigned a conservative tracer concentration of 1000 mg/L and 0 mg/L, respectively, for calculation of mixing fractions and REN. The advection, dispersion, and source-sink mixing packages were used; diffusion and density effects were assumed to be negligible. A longitudinal dispersivity value of 5m was calculated using the maximum flow length of the model domain using Equation 5; this value agrees with previous studies of similar scale (Fatkhutdinov & Stefan, 2019; Forghani & Peralta, 2018; Ward et al., 2009). Horizontal and vertical transverse dispersivites were set to 0.5m and 0.05m, respectively. The Total Variation Diminishing (TVD) solver was used for the advection package to minimize numerical dispersion and artificial oscillation.

2.4 Reactive Transport Model Setup

Based on preliminary analysis of conservative transport results, a reactive transport model was developed . Due to this, reactive transport models of all storage durations and pumping rate combinations with a specific discharge of 0.025 were run to determine the effect of variable pumping rates and storage durations on pyrite oxidation and arsenic behavior.

Reactive transport was modeled using PHT3D, which links the chemical reaction capabilities of PHREEQC with the flow and transport capabilities of MODFLOW/MT3DMS (Appelo & Rolle, 2010). Initial concentrations of mobile species and minerals for ambient groundwater and injected water were modeled after Wallis et al. (2011) and are given in Table 3, except for the weight percentage of arsenic included in pyrite, which was adjusted to 0.4% following Antoniou et al. (2015). Pyrite was assumed to have a homogenous distribution in the aquifer. Pyrite oxidation is the only kinetic reaction considered in the model and uses the

reaction equation of Williamson & Rimstidt (1994) (Antoniou et al., 2015; Wallis et al., 2011). The WATEQ4F database, included with PHREEQC, was used with minor modifications to allow for arsenic release following pyrite oxidation (Appendix B). The PHREEQC-2 interface package file is given in Appendix C.

Sorption of arsenic onto HFO was modeled using surface data from Dzombak & Morel (1990) (Antoniou et al., 2015; Lazareva et al., 2015; Wallis et al., 2011), which is included in the default WATEQ4F database. Weak and strong sorption sites were linked to the mass of HFO and were assigned values of 0.2 and 0.005 sites/mol HFO, respectively (Antoniou et al., 2015; Dzombak & Morel, 1990; Wallis et al., 2011). A surface area of 5.33×10^4 m^2/mol Fe was used which is consistent with previous studies (Antoniou et al., 2015; Dzombak & Morel, 1990). Cation exchange was modeled using initial exchanger compositions from Wallis et al. (2011); this allows for competitive sorption of cations on HFO.

Due to the increased computational demand required for reactive transport simulations, the model domain was simplified to 1500 m parallel to flow by 250 m perpendicular to flow; this domain allows for tracking of resultant plumes downgradient and decreased computation time without the intersection of boundary conditions and resultant plumes. In addition to the simplification of the model domain with respect to the conservative transport model domain, the vertical discretization of the reactive transport models was decreased to one layer. As the hypothetical aquifer simulated in this study is homogeneous and density effects are assumed to be negligible, the use of a single layer is justified (Anderson et al., 2015; Prommer et al., 2018). Simplifying the vertical discretization drastically reduced run-times and, in the case of conservative transport, has negligible impact on model output (Forghani et al. 2017).

Table 3. Ambient and Injected Water Concentrations for Reactive Transport Model.

Species	Ambient Groundwater (mmol/L)	Injected Water (mmol/L)
As	0	0
C(4)	2.38	1.04
C(-4)	7.80E-06	0
Ca	5.24	1.1
Cl	1	0.91
Fe(2)	0	0
Fe(3)	0	0
K	0.098	0.049
Mg	3.2	0.354
Na	1.09	2
O(0)	0	3.60E-04
S(-2)	1.80E-02	0
S(6)	7.4	1.56
pH	7.3	7.7
pe	-3.7	13
As-pyrite	0.018	
Calcite	0.53	
$Fe(OH)_3(a)$	0	
CaX2	0.0181	
MgX2	6.60E-03	
NaX	2.90E-04	
KX	1.30E-04	
FeX2	0.00E+00	

3. RESULTS AND DISCUSSION

3.1 Conservative Transport Models

3.1.1 Effect of altering pumping rates on system performance

Conservative transport results indicated cumulative REN and mixing fractions at the well were higher for lower values of hydraulic gradient and shorter storage periods (Appendix D), which is consistent with previous studies' findings on system performance (Forghani & Peralta, 2018; Lowry & Anderson, 2006; Ward et al., 2009). However, while system performance is lower for simulations with higher gradients and longer storage durations, the variability of system performance due to pumping rates was greater in these situations (Appendix D). For hydraulic gradients of 0.0001 and 0.001, variability in cumulative REN compared to the baseline pumping scenario ranged from <1% to ~1.3% (Appendix D), which is equivalent to a maximum of 40,950 m^3 more injected water recovered over a ten-year span. For hydraulic gradients of 0.0025 and 0.005, however, variability in cumulative REN compared to the baseline scenario ranged from ~2.4% to 5% (Appendix D). In the context of these simulations, an improvement of 5% in cumulative REN is equivalent to ~158,000 m^3 more injected water recovered over a ten-year span.

Mixing fractions followed a similar trend to cumulative REN with respect to hydraulic gradient and storage duration (Figures 1-3). Improvements in mixing fraction compared to the baseline pumping scenario ranged from <1% to ~23% for hydraulic gradients of 0.0001 and 0.005, respectively. Higher mixing fractions indicate less mixing is occurring, which has implications for chemical reactions between waters with different chemical compositions, as discussed in section 3.2.

Increasing either the injection or extraction rate resulted in higher system performance for all combinations of storage durations and gradients considered, and vice versa; although, this difference may be negligible (as small as ~0.2%) for some combinations of hydraulic gradient and storage duration as discussed previously. System performance was more sensitive to extraction rates than injection rates, as the fast and slow extraction scenarios resulted in the maximum and minimum mixing fraction and cumulative REN, respectively, for each combination of storage period and hydraulic gradient. These results are consistent with Forghani & Peralta (2018), who found ASR system performance to be positively correlated with injection rate and the ratio of extraction rate to injection rate.

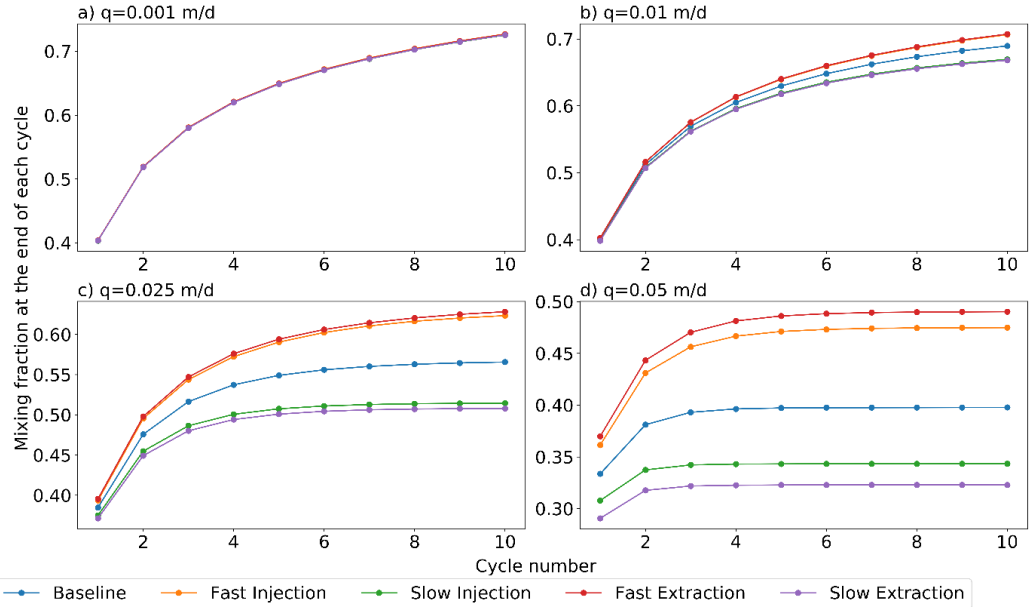

Figure 1. Mixing fraction at the end of each cycle with a zero-day storage duration shown for a specific discharge of a) q=0.001 m/d, b) q=0.01 m/d, c) q=0.025 m/d, d) q=0.05 m/d.

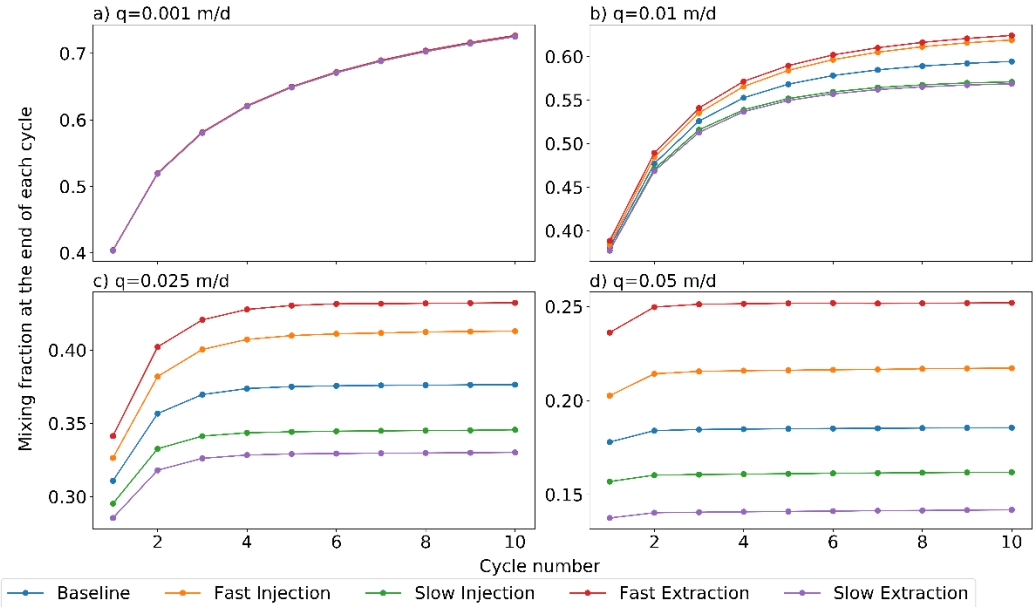

Figure 2. Mixing fraction at the end of each cycle with a six-month storage duration shown for a specific discharge of a) q=0.001 m/d, b) q=0.01 m/d, c) q=0.025 m/d, d) q=0.05 m/d.

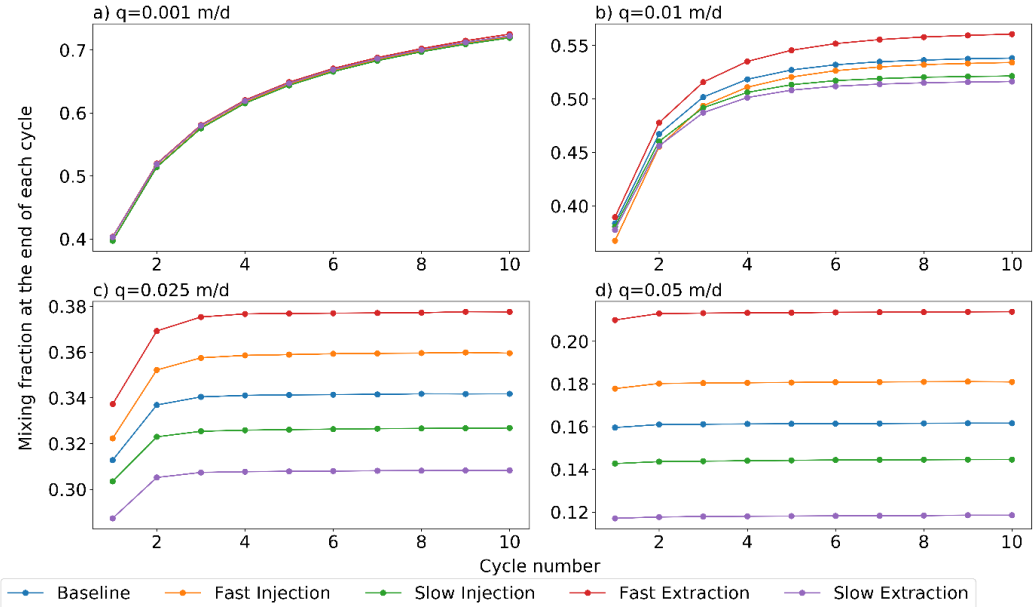

Figure 3. Mixing fraction at the end of each cycle with a one-year storage duration shown for a specific discharge of a) q=0.001 m/d, b) q=0.01 m/d, c) q=0.025 m/d, d) q=0.05 m/d.

3.2 Reactive Transport Models

3.2.1 Effect of Storage Duration

Longer storage durations result in higher arsenic concentrations at the well and more mobilized arsenic overall (Figure 4); the total mass of non-sorbed arsenic in the aquifer at the end of the simulation for the one-year storage duration is more than double that of the zero-day storage simulation (Appendix E). Increasing the storage duration increases the amount of arsenic released in two ways: more dissolved HFO and longer residence time of dissolved oxygen. A longer storage duration allows more time for ambient reducing groundwater to flow towards the well and dissolve HFO, subsequently releasing sorbed arsenic; this dissolution can be seen at the end of extraction for the six-month and one-year storage durations, but not the zero-day storage duration (Appendix G). When there is no storage duration and extraction begins immediately after the end of injection, approximately 40% more oxygen is removed by the well. Less oxygen present results in less pyrite dissolved, less arsenic mobilized, and lower arsenic concentrations at the well.

While arsenic concentrations eventually decrease below the MCL over multiple cycles for the zero-day storage and six-month storage scenarios, arsenic concentrations above the EPA's MCL of 10 μg/L persist for multiple cycles of the one-year storage scenario. This is due to the degree of HFO dissolution in the one-year storage simulations (Appendix E) and the amount of pyrite dissolved. The gradual increase of HFO that occurs in the shorter storage duration simulations, which is consistent with previous studies (Antoniou et al., 2015; Wallis et al., 2011), is hindered by the greater degree of HFO dissolution in the one-year storage duration. In addition, more oxygen is used for pyrite dissolution in the one-year storage duration scenario.

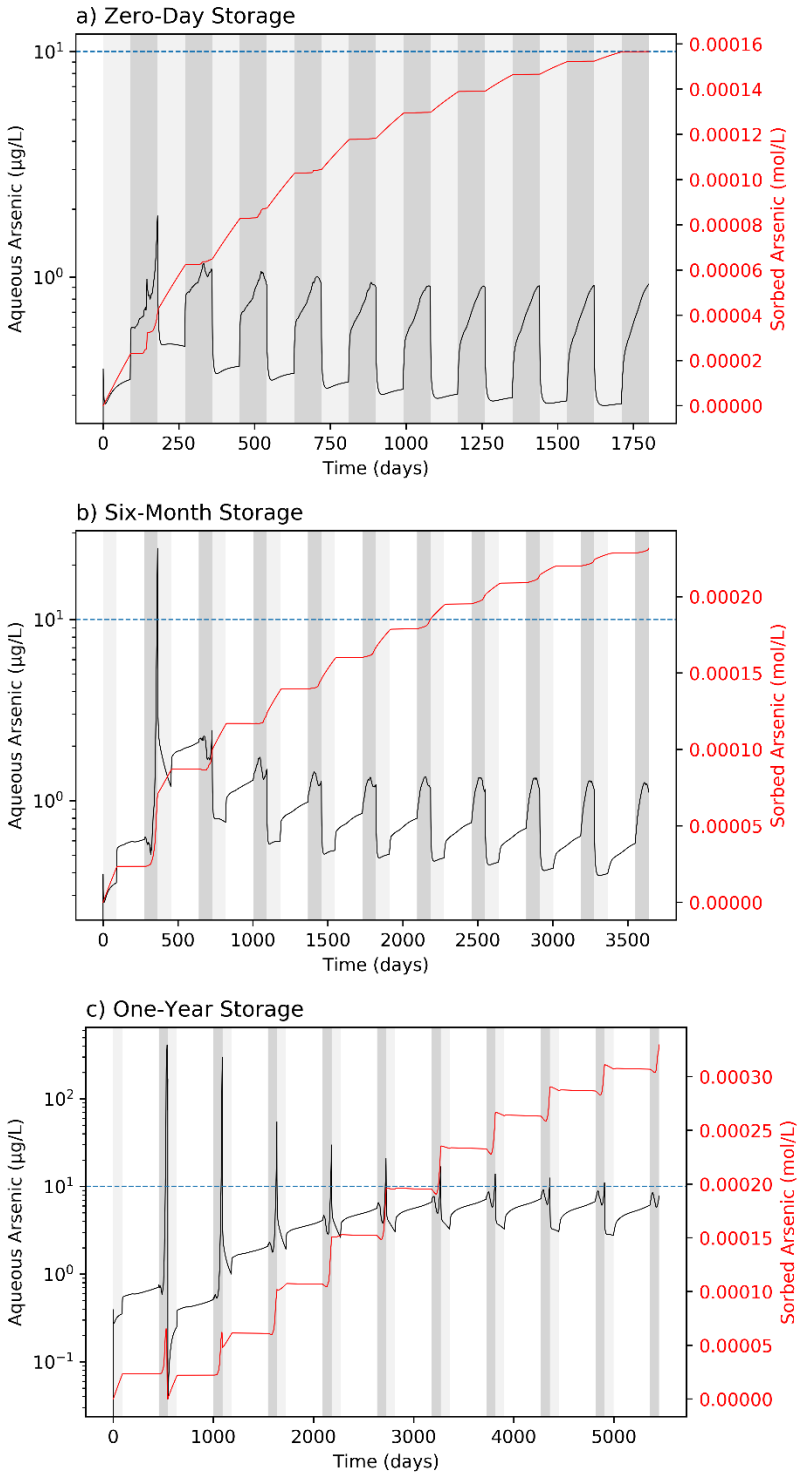

Figure 4. Aqueous (black) and sorbed (red) arsenic concentrations vs. time for the baseline pumping scenario for all storage durations. The arsenic MCL is represented by the dotted blue line. Shaded areas represent injection (light gray), storage (white), and extraction (dark gray).

3.2.2 Effect of Injection Rates

3.2.2.1 Effect on DO, pyrite oxidation, and HFO precipitation

Larger injection rates result in a larger spatial extent of DO around the well at the end of injection (i.e., the DO front is further from the well), which alters the spatial extent of pyrite oxidation and HFO precipitation as well (Figure 5). DO affects the redox zonation around the well at the end of storage. As DO is used during storage the redox conditions in the aquifer shift back to reducing. This results in a smaller oxidizing area around the well for the slow injection scenario.

The end of cycle 1 injection is shown in Figure 5, but the trend persists for all subsequent cycles. Despite the larger spatial extent of pyrite oxidation in the fast injection scenario, more pyrite is oxidized in the slow injection scenario (Figure 5). Because more pyrite is dissolved in the slow injection scenario, more Fe(II) is introduced to solution, which is further oxidized to precipitate HFO. The spatial extent of HFO around the well follows the same trend as DO and pyrite oxidation, which affects the location of mobilized arsenic. Arsenic is mobilized on the edge of the DO front because less DO is present for arsenic oxidation and precipitation of HFO (Antoniou et al., 2017).

3.2.2.2 Effect on recovered, aqueous, and sorbed arsenic concentrations

Average recovered arsenic concentrations per cycle are initially above the EPA's MCL at the end of cycle 1 for all values of injection rate considered but meet the MCL for subsequent cycles (Figure 6). Lower injection rates result in higher recovered arsenic concentrations for all cycles. Due to the smaller spatial extent of pyrite oxidation around the well for the slow injection scenario, non-sorbed arsenic concentrations are closer to the well at the beginning of extraction. The closer proximity of mobilized arsenic results in the elevated recovered arsenic

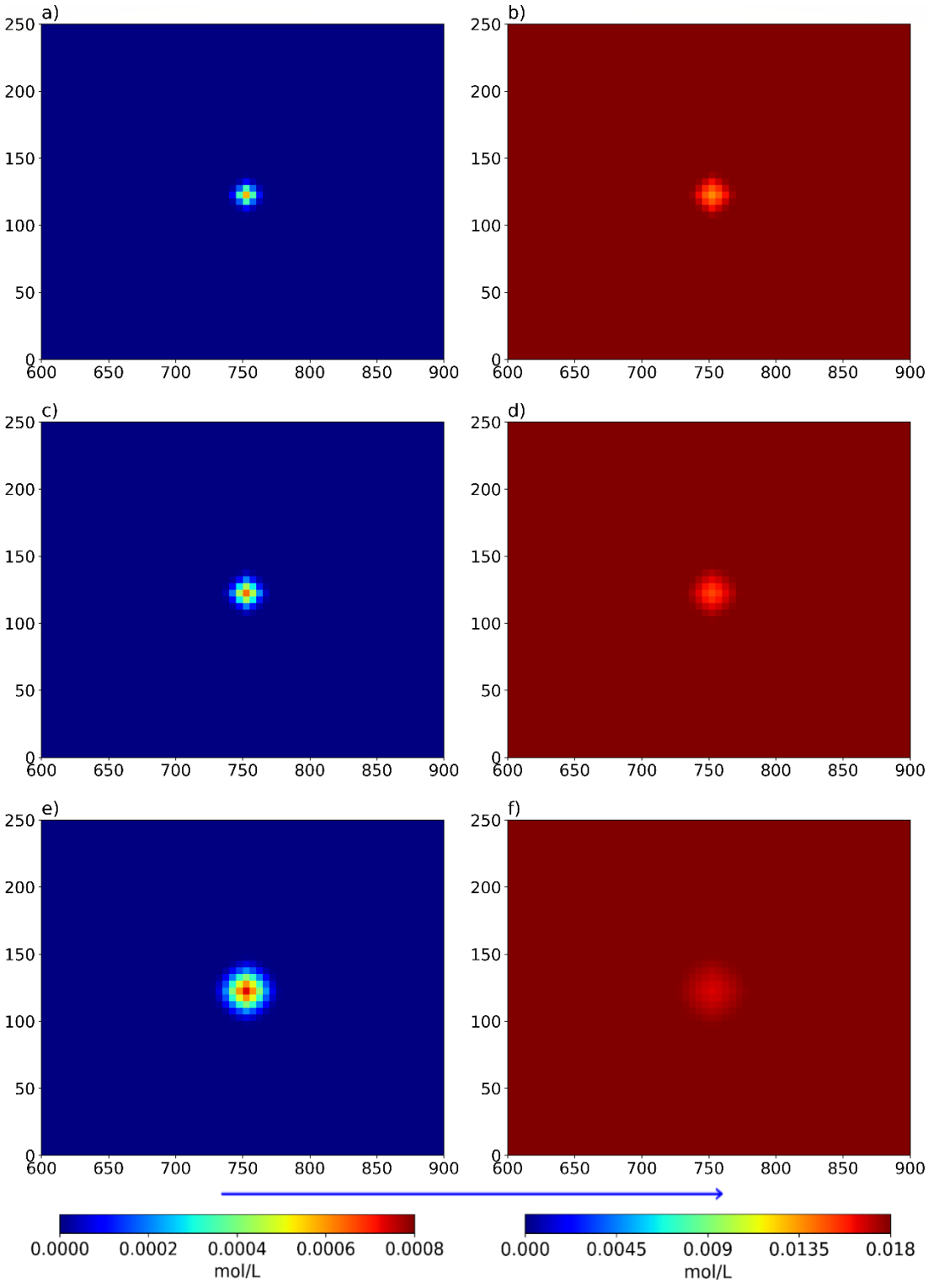

Figure 5. Dissolved oxygen (a, c, e) and pyrite (b, d, f) concentrations at the end of first injection for slow injection (Row 1), baseline (Row 2), and fast injection (Row 3) scenarios with a six-month storage duration. The arrow indicates the direction of the hydraulic gradient.

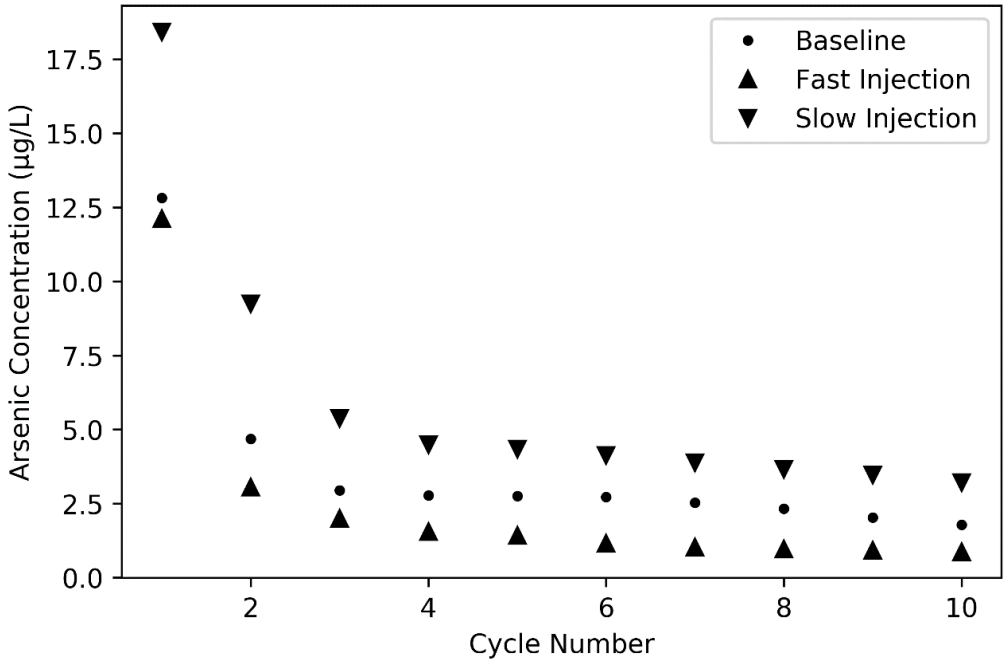

Figure 6. Average recovered arsenic concentrations per cycle for the baseline, fast injection, and slow injection scenarios.

concentrations. Although recovered arsenic concentrations meet the MCL for all cycles after the first, they do not meet the arsenic MCLG, which may still cause health effects.

Aqueous arsenic concentrations at the well are above the EPA's MCL at the end of the first cycle for all injection rates, although the magnitude is greater for the fast injection scenario than for the slow injection scenario (Figure 7). The peak in arsenic concentration at the end of the first extraction represents the release of arsenic from HFO as redox conditions change. This peak in concentration gradually declines as HFO concentrations increase over time. This difference is likely due to the greater recovered arsenic in the slow injection scenario; due to the proximity of the DO front, more arsenic is recovered in the slow injection scenario, which leaves less arsenic at the well. In subsequent cycles, however, arsenic concentrations at the well remain below the MCL.

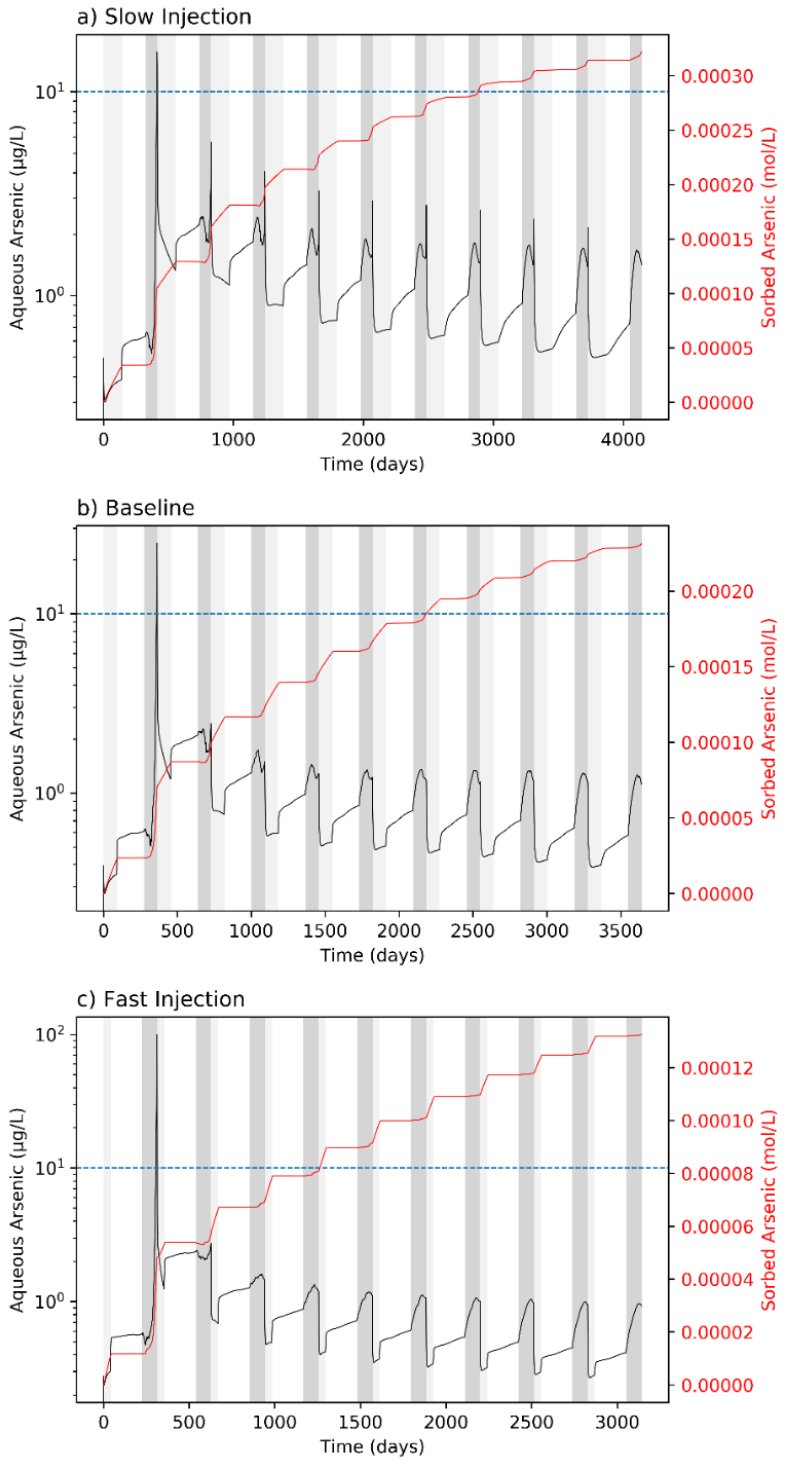

Figure 7. Aqueous and sorbed arsenic concentrations at the well vs. time for the slow injection, baseline, and fast injection scenarios with a six-month storage duration. The arsenic MCL is represented by the dotted blue line. Shaded areas represent injection (light gray), storage (white), and extraction (dark gray).

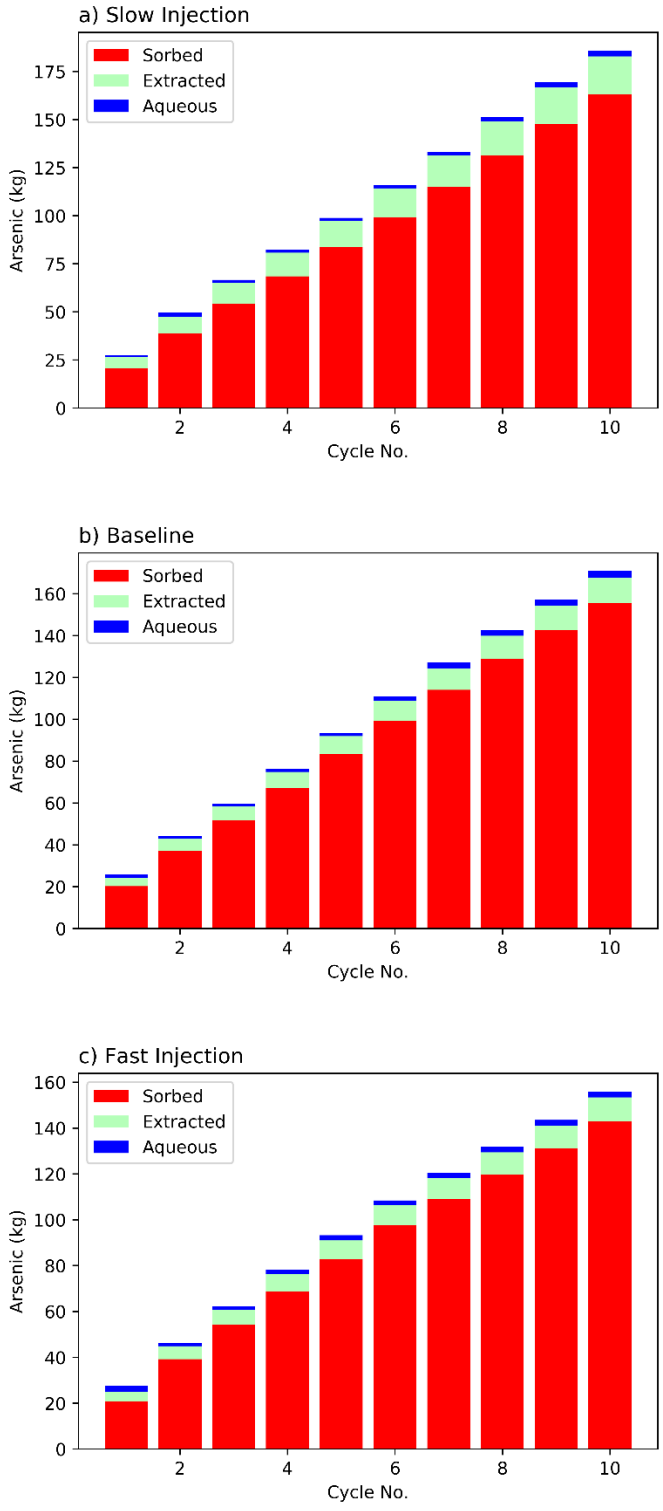

Figure 8. Total arsenic released via pyrite oxidation separated into sorbed, extracted, and aqueous mass for the slow injection, baseline, and fast injection scenarios.

Sorbed arsenic concentrations at the well are greater for the slow injection scenario than for the fast injection scenario, which agrees with greater HFO concentrations (Appendix E). Because HFO concentrations, and therefore sorbed arsenic concentrations, are lower for the fast injection scenario, arsenic remains mobile and results in the elevated concentrations seen at the end of the first cycle (Figure 6). However, arsenic concentrations at the well for subsequent cycles in the fast injection scenario are lower than for the slow injection scenario. While there is increased sorption of arsenic on HFO in the slow injection scenario, the amount of arsenic released via pyrite oxidation is greater with lower injection rates (Figure 8).

3.2.3 Effect of Extraction Rates

Given a constant injection rate, higher extraction rates generally resulted in lower average recovered arsenic concentrations, except for the first cycle, and vice versa (Figure 9). This behavior of arsenic in response to extraction rates is consistent with previous studies, although these studies were for extraction-only wells that found increased extraction rates resulted in higher arsenic concentrations in water-supply wells, although this was at least in part due to seasonal variability and these studies did not consider ASR wells (Bexfield & Jurgens, 2014; Degnan et al., 2020; Wallis et al. 2011). Compared to the baseline pumping scenario, ~10% more or less arsenic was mobilized via pyrite dissolution for the slow and fast extraction pumping scenario, respectively, over the entire simulation (Figure 10). This difference in the amount of mobilized arsenic contributed to differences in recovered arsenic concentrations, with ~25% more and ~16% less arsenic recovered during extraction compared to the baseline scenario for the slow extraction and fast extraction scenarios, respectively.

Altering the extraction rates affects arsenic concentrations in two ways: oxygen removal

and HFO precipitation. The fast extraction scenario is 100 days shorter than the slow extraction scenario, which allows less time for oxygen to dissolve pyrite and release arsenic and results in approximately four times as much oxygen being recovered from the well compared to the slow extraction scenario. In addition to enhanced oxygen removal and less mobilized arsenic, the fast

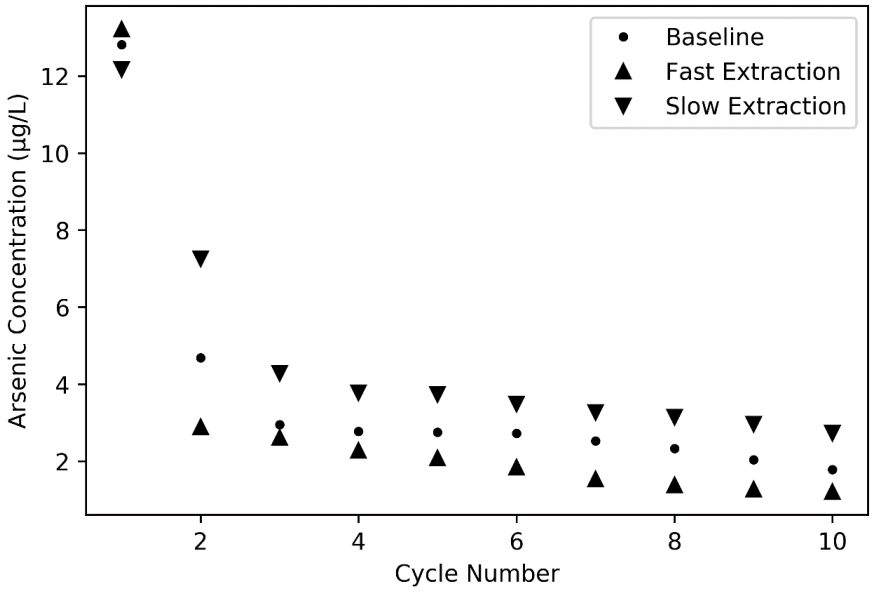

Figure 9. Average recovered arsenic concentrations per cycle for the baseline, fast extraction, and slow extraction scenarios.

extraction scenario allows less time for the injected water to migrate due to the hydraulic gradient compared to the slow extraction scenario. Altering the extraction rate affects the HFO distribution spatially and temporally. Near the end of extraction, as ambient reducing groundwater is nearing the well, a larger amount of HFO dissolves during the slow extraction scenario than the fast extraction scenario (Appendix G). This dissolution of HFO results in

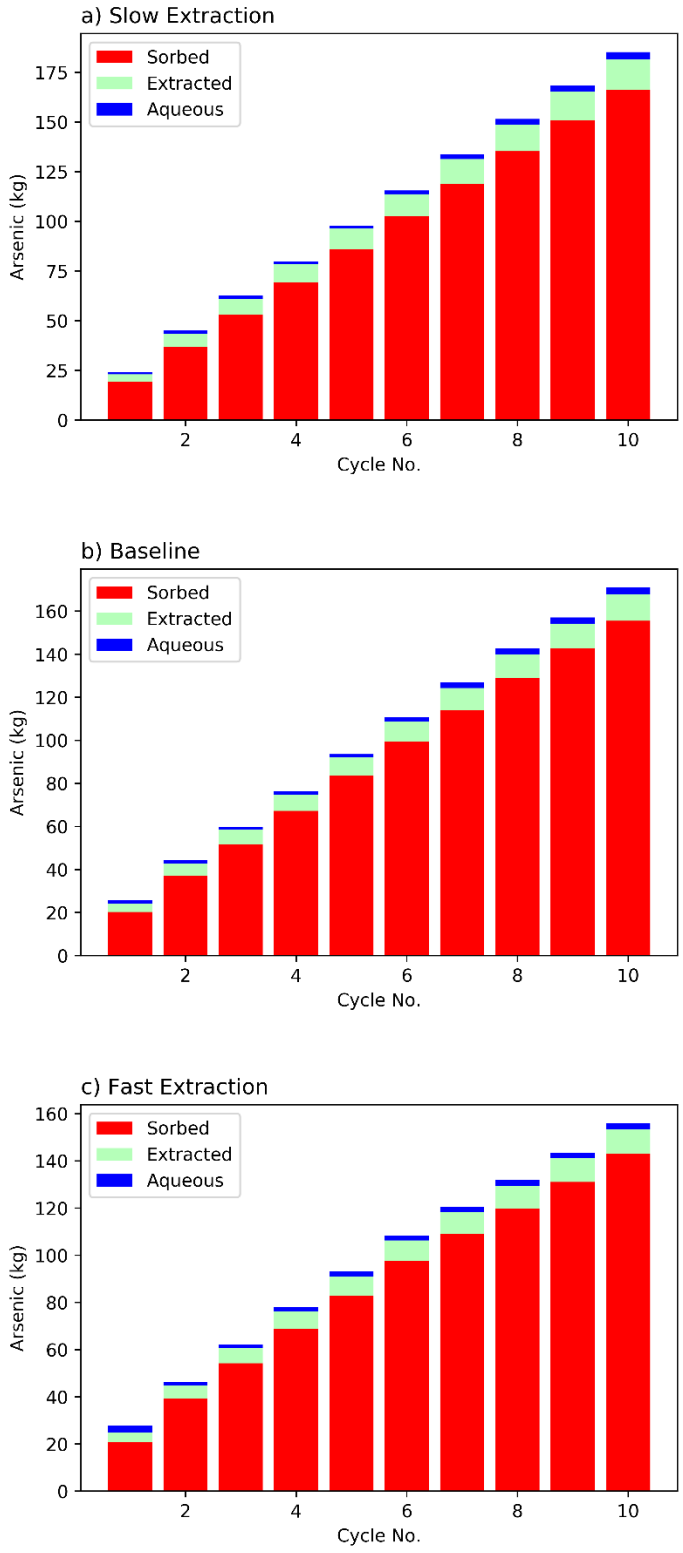

Figure 10. Total arsenic released via pyrite oxidation separated into sorbed, extracted, and aqueous mass for the slow injection, baseline, and fast injection scenarios.

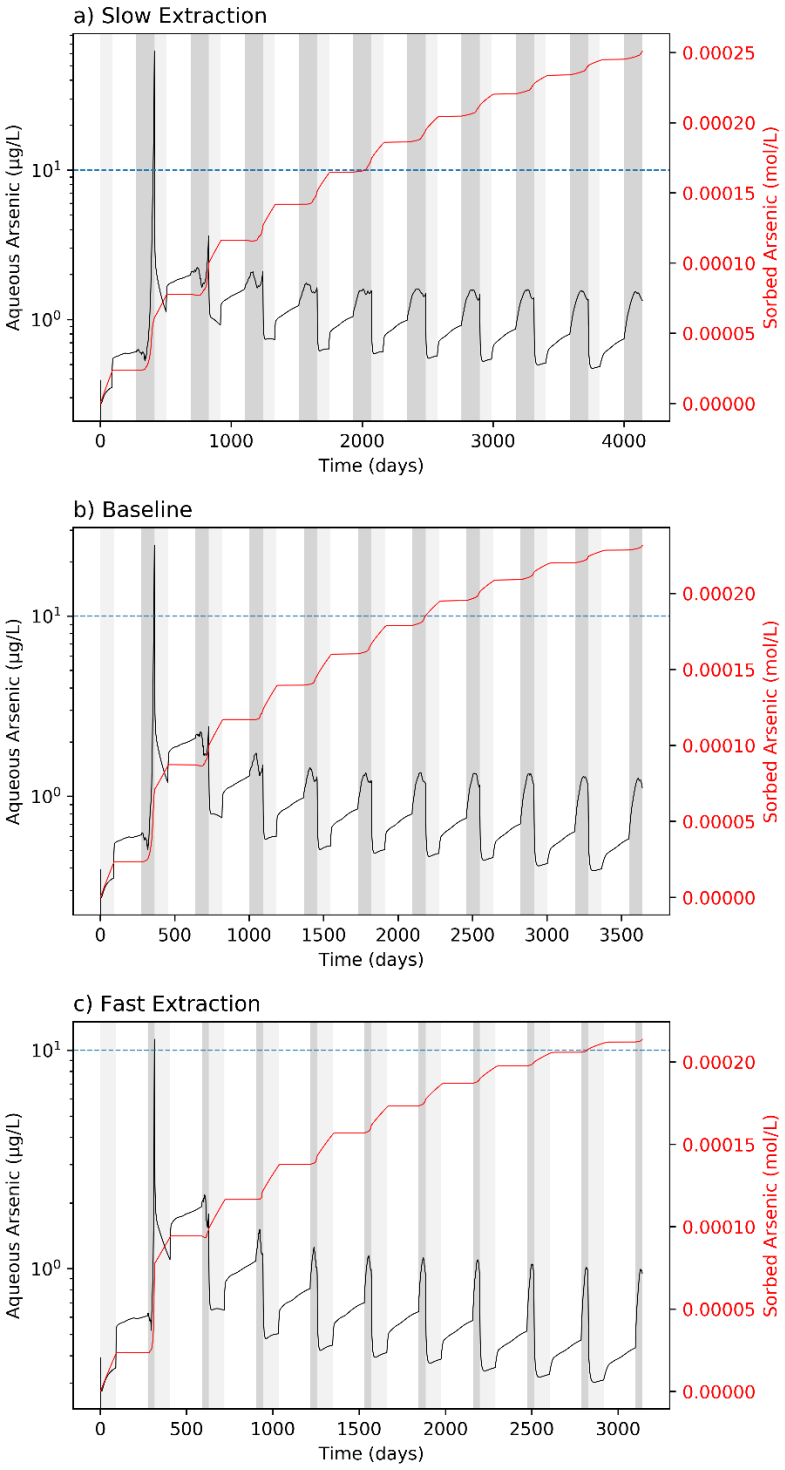

Figure 11. Aqueous and sorbed arsenic concentrations vs. time for the slow extraction, baseline, and fast extraction pumping scenarios with a six-month storage duration. The arsenic MCL is represented by the dotted blue line. Shaded areas represent injection (light gray), storage (white), and extraction (dark gray).

higher arsenic concentration at the well (Figure 11). In later cycles of the fast extraction scenario, HFO precipitates further upgradient of the well than in the slow extraction scenario, which keeps sorbed arsenic further from the well. Altering the extraction rates also affects the amount of HFO precipitated, with ~12% more HFO precipitated in the fast extraction scenario compared to the slow extraction scenario.

3.2.4 Unrecovered Arsenic

By the end of the simulation for all storage periods and pumping scenarios considered, arsenic concentrations downstream of the ASR well are elevated beyond the native concentration of 0 µg/L (Figure 12). The release of arsenic downstream is because the full injected volume is recovered each cycle, which shifts the redox conditions around the well back to reducing, dissolving some, but not all, HFO and releasing sorbed arsenic. While this behavior of HFO has been acknowledged in previous studies, they did not consider an ASR operation on the scale of the one considered in this study or the long-term spatial extent of arsenic. For the six-month storage period, depending on the pumping scenario, ~2.6 – 3.7 kg of arsenic were released downstream and not subsequently recovered by the well or sorbed onto HFO, which has negative implications for downgradient users. This effect could be magnified for large-scale multi-well ASR systems but testing this is beyond the scope of the present study.

In addition to the large plume of unrecovered arsenic moving downstream, there is also a smaller area upgradient of the well with arsenic concentrations above the EPA's MCL (Figure 12). This area forms at the end of every extraction due to dissolution of HFO, but it does not result in significant migration, because injection immediately follows the end of extraction, which shifts the redox conditions back to oxidizing, causing arsenic to resorb to HFO. If,

however, extraction was to continue once the injected volume had been recovered, recovered arsenic concentrations would be above the MCL.

Real ASR systems will not follow an exact schedule as the one simulated in this study, as schedules are usually dictated by supply and demand; if an ASR operation were to cease for a period of time following an extraction of the full injection volume, the elevated arsenic concentrations would be free to migrate downgradient. To test this, a model with the baseline pumping scenario and a six-month storage period was run for ten years after the first cycle to show the migration of arsenic under the hydraulic gradient. Results show the plume of elevated arsenic will migrate downstream following the cessation of ASR operations (Figure 13). It is important to note that the only arsenic attenuation process considered in this reaction network is sorption onto HFO. However, mobile arsenic concentrations may also decrease through the precipitation of arsenic-containing minerals in reducing conditions such as scorodite, orpiment, and realgar (Neil et al., 2012). Whether this would be an appreciable attenuation mechanism for the arsenic plume in Figure 11 is beyond the scope of the present work.

The results shown in Figure 13 imply that extra precaution must be taken when performing ASR with oxygenated water in an aquifer containing arsenic-bearing pyrite. If an ASR operation is to be shut down, cease operations indefinitely, or if cycle testing is being performed, reactive transport models should be run to ensure there is no likelihood of arsenic being released downgradient. Deoxygenation of water prior to injection has been shown to decrease arsenic concentrations and may allow for ASR in aquifers containing arsenic-bearing pyrite (Prommer, 2018). If water isn't deoxygenated prior to injection, an oxidizing plume around the well should be maintained to prevent downgradient migration.

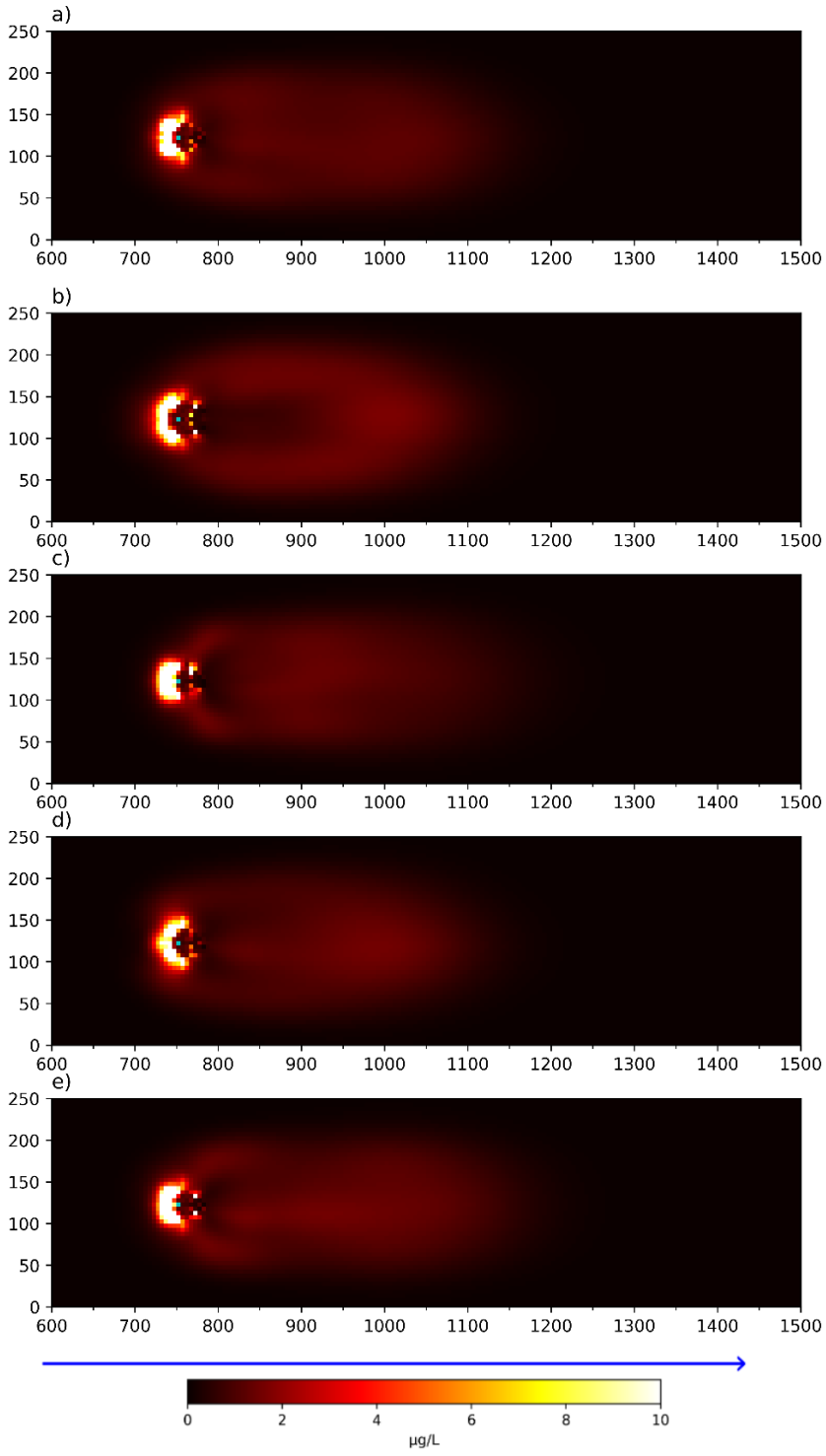

Figure 12. Arsenic concentrations at the end of simulation with six-month storage for: a) baseline, b) fast injection, c) slow injection, d) fast extraction, and e) slow extraction pumping scenarios. The blue cell represents the ASR well. The blue arrow indicates the direction of the hydraulic gradient.

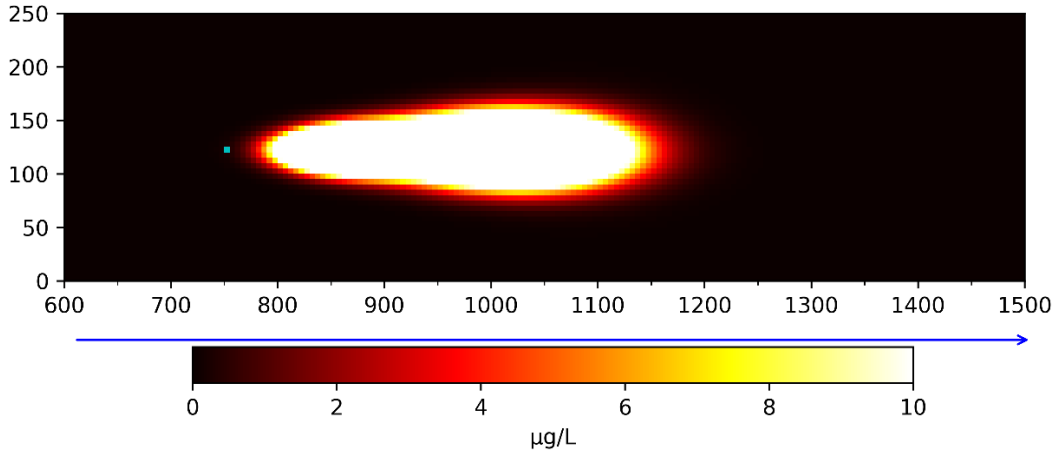

Figure 13. Arsenic concentration ten years after one cycle for the baseline pumping scenario with a storage period of six months. The blue cell represents the ASR well, and the blue arrow represents the direction of the hydraulic gradient.

4. CONCLUSIONS

For a fixed volume of water, increasing the injection or extraction rate of a hypothetical ASR system results in better system performance, and vice versa. This improvement in system performance compared to lower pumping rates can initially be small but increases over multiple cycles, with up to ~158,000 m^3 more injected water recovered over a ten-year period. Little improvement in system performance should be expected in areas with low hydraulic gradients (on the order of 0.0001); however, there is a greater variability in system performance with respect to pumping rate for situations with larger gradients or longer storage times. If altering pumping rates is feasible for a specific ASR system, this variability in system performance indicates increasing pumping rates may be a viable method of increasing system performance, especially over long periods of time.

In addition to affecting system performance in conservative transport scenarios, altering the pumping rates also affects recovered arsenic concentrations and the magnitude of arsenic released via pyrite dissolution. Injection rates affect the spatial distribution of dissolved oxygen around the well, with higher injection rates resulting in a larger dissolved oxygen plume, and vice versa. This difference in the extent of the dissolved oxygen plume indicates altering the injection rates can be used to control the distance at which arsenic is mobilized but not subsequently sorbed to hydrous ferric oxides. Controlling the location of the dissolved oxygen front may be useful in preventing unwanted arsenic migration downgradient.

Extraction rates have the greatest influence on the amount of arsenic mobilized, due to a decreased residence time of dissolved oxygen in the aquifer. This effect of extraction rates on mobilized arsenic underscores the importance of controlling dissolved oxygen in aquifers containing arsenic-bearing pyrite. While decreasing residence time of dissolved oxygen via

increased extraction rates results in less mobilized arsenic, deoxygenation prior to injection should be the preferred method if feasible.

The framework of this study led to the unprecedented, but unsurprising, result of arsenic migration downstream outside of the well's capture zone. While a real ASR system is unlikely to operate in the same way as the one modeled in this study (i.e., extracting the full injected volume each cycle), these results highlight some long-term risks associated with performing ASR in aquifers containing arsenic-bearing pyrite. If a buffer zone is built and maintained properly, then there is little to no risk of arsenic migration as seen in this study. However, if unforeseen circumstances were to disrupt the operations, or if the ASR system were to permanently cease operations, the issue of the sorbed arsenic would need to be addressed, lest it result in downstream migration and negatively impact downstream users or the environment. While ASR systems can operate and maintain acceptable recovered arsenic concentrations in aquifers containing arsenic-bearing pyrite, the sorption of arsenic on HFO is metastable and should be a going concern. Deoxygenation of water prior to injection presents additional cost but prevents the possibility of arsenic migration to the degree seen in this study.

REN is not a widely used metric of system performance and most operators are likely to use RE to determine system performance. Until recently, limitations of modeling software prevented termination of pumping once a certain concentration is reached. However, the contaminant treatment system package included with MT3D-USGS may be used to achieve this goal. Proper implementation of this package in conservative transport scenarios can be used to simulate the effect altered pumping rates on RE, which may be of more use to ASR operators. While some aquifers can be modeled as one homogeneous layer, the addition of physical heterogeneity may more accurately represent some ASR systems and reveal issues associated

with high transmissivity zones and reactive transport. The author is unaware of any studies to date on the interplay of multiple wells in an ASR wellfield in the context of reactive transport. The larger plume of injected water would result in more arsenic released, which could result in more arsenic released downstream. Finally, the minimum grid size in reactive transport models was limited by the software. Parallelization has been used for other reactive transport codes, resulting in decreased run times for complex models, but has not yet been implemented for PHREEQC or PHT3D. Parallelization of PHT3D may make a more refined grid and thus more accurate solutions possible.

REFERENCES

Ahani Amineh, Z. B., Hashemian, S. J. A. D., & Magholi, A. (2017). Integrating Spatial Multi Criteria Decision Making (SMCDM) with Geographic Information Systems (GIS) for delineation of the most suitable areas for aquifer storage and recovery (ASR). *Journal of Hydrology, 551*, 577-595. https://doi.org/10.1016/j.jhydrol.2017.05.031

Anderson, M.P., Woessner, W.W. and Hunt, R.J., 2015. Applied groundwater modeling: simulation of flow and advective transport. Academic press.

Antoniou, E. A., van Breukelen, B. M., Putters, B., & Stuyfzand, P. J. (2012). Hydrogeochemical patterns, processes and mass transfers during aquifer storage and recovery (ASR) in an anoxic sandy aquifer. *Applied Geochemistry, 27*(12), 2435-2452. https://doi.org/10.1016/j.apgeochem.2012.09.006

Antoniou, E. A., van Breukelen, B. M., & Stuyfzand, P. J. (2015). Optimizing aquifer storage and recovery performance through reactive transport modeling. *Applied Geochemistry, 61*, 29-40. https://doi.org/10.1016/j.apgeochem.2015.05.009

Antoniou, A., Smits, F., & Stuyfzand, P. (2017). Quality assessment of deep-well recharge applications in the Netherlands. *Water Science and Technology: Water Supply, 17*(5), 1201-1211. https://doi.org/10.2166/ws.2017.032

Appelo, C. A., & Rolle, M. (2010). PHT3D: A reactive multicomponent transport model for saturated porous media. *Ground Water, 48(5),* 627-632. https://doi.org/10.1111/j.1745-6584.2010.00732.x

Bakker, M. (2010). Radial Dupuit Interface Flow to assess the aquifer storage and recovery potential of saltwater aquifers. *Hydrogeology Journal, 18*(8), 107–115. https://doi.org/10.1007/s10040-009-0508-1

Bakker, M., Post, V., Langevin, C. D., Hughes, J. D., White, J. T., Starn, J. J., & Fienen, M. N. (2016). Scripting MODFLOW Model Development Using Python and FloPy. *Groundwater, 54*(5), 733-739. https://doi.org/10.1111/gwat.12413

Bedekar, V., Morway, E.D., Langevin, C.D., and Tonkin, M. (2016), MT3D-USGS version 1: A U.S. Geological Survey release of MT3DMS updated with new and expanded transport capabilities for use with MODFLOW: U.S. Geological Survey Techniques and Methods 6-A53, 69 p., https://doi.org/10.3133/tm6A53

Bexfield, L. M., & Jurgens, B. C. (2014). Effects of seasonal operation on the quality of water produced by public-supply wells. *Ground Water, 52 Suppl 1*, 10-24. https://doi.org/10.1111/gwat.12174

Brown, C. J., Ward, J., & Mirecki, J. (2016). A Revised Brackish Water Aquifer Storage and Recovery (ASR) Site Selection Index for Water Resources Management. *Water Resources Management, 30*(7), 2465-2481. https://doi.org/10.1007/s11269-016-1297-7

Ceric, A., & Haitjema, H. (2005). On Using Simple Time-of-Travel Capture Zone Delineation Methods. *Groundwater, 43*(3), 408-412. https://doi.org/10.1111/j.1745-6584.2005.0035.x

Davis, A. D. (1986). Deterministic modeling of dispersion in heterogeneous permeable media. *Groundwater, 24*(5), 609-615. https://doi.org/10.1111/j.1745-6584.1986.tb03709.x

Degnan, J. R., Levitt, J. P., Erickson, M. L., Jurgens, B. C., Lindsey, B. D., & Ayotte, J. D. (2020). Time scales of arsenic variability and the role of high-frequency monitoring at three water-supply wells in New Hampshire, USA. *Sci Total Environ, 709*, 135946. https://doi.org/10.1016/j.scitotenv.2019.135946

Dillon, P. (2005). Future management of aquifer recharge. *Hydrogeology Journal, 13*(1), 313-316. https://doi.org/10.1007/s10040-004-0413-6

Dillon, P., Pavelic, P., Page, D., Beringen, H., & Ward, J. (2009). *Managed aquifer recharge: An Introduction.*

Drewes, J. E. (2009). Ground Water Replenishment with Recycled Water-Water Quality Improvements during Managed Aquifer Recharge. *Groundwater, 47*(4), 502-505. https://doi.org/10.1111/j.1745-6584.2009.00587_5.x

Dzombak, D. A.; Morel, F. M. M. Surface Complexation Modeling; Wiley and Sons: New York, 1990.

Fatkhutdinov, A., & Stefan, C. (2019). Multi-Objective Optimization of Managed Aquifer Recharge. *Groundwater, 57*(2), 238–244. https://doi.org/10.1111/gwat.12793

Forghani, A., & Peralta, R. C. (2017). Transport modeling and multivariate adaptive regression splines for evaluating performance of ASR systems in freshwater aquifers. *Journal of Hydrology, 553*, 540-548. https://doi.org/10.1016/j.jhydrol.2017.08.012

Forghani, A., & Peralta, R. C. (2018). Intelligent performance evaluation of aquifer storage and recovery systems in freshwater aquifers. *Journal of Hydrology, 563*, 599-608. https://doi.org/10.1016/j.jhydrol.2018.06.042

Guo, W., Coulibaly, K., & Maliva, R. G. (2014). Simulated effects of aquifer heterogeneity on ASR system performance. *Environmental Earth Sciences, 73*(12), 7803-7809. https://doi.org/10.1007/s12665-014-3822-4

Harbaugh, A.W. (2005). MODFLOW-2005, the U.S. Geological Survey modular ground-water model -- the Ground-Water Flow Process: U.S. Geological Survey Techniques and Methods 6-A16. https://doi.org/10.3133/tm6A16

Harpaz, Y., & Bear, J. (1964). Investigation on mixing of waters in underground storage operations, International Association of Scientific Hydrology, Commission of Subterranean Waters, Publication 64, pp. 132–153.

Heath, R. C. (1983). *Basic ground-water hydrology* (2220). Retrieved from Reston, VA: http://pubs.er.usgs.gov/publication/wsp2220

Helfer, Fernanda, Charles Lemckert, and Hong Zhang. 2012. Impacts of climate change on temperature and evaporation from a large reservoir in Australia. *Journal of Hydrology* 475: 365-378. https://doi.org/10.1016/j.jhydrol.2012.10.008

Jeong, Hoon Young, Seong-Chun Jun, Jeong-Yong Cheon, and Minji Park. 2018. A review on clogging mechanisms and managements in aquifer storage and recovery (ASR) applications. *Geosciences Journal*, 22(4), 667-679. https://doi.org/10.1007/s12303-017-0073-x

Jones, G. W., & Pichler, T. (2007). Relationship between pyrite stability and arsenic mobility during aquifer storage and recovery in southwest central Florida. *Environmental Science and Technology, 41*(3), 723-730. https://doi.org/10.1021/es061901w

Khan, S., Mushtaq, S., Hanjra, M. A., & Schaeffer, J. (2008). Estimating potential costs and gains from an aquifer storage and recovery program in Australia. *Agricultural Water Management, 95*(4), 477-488. https://doi.org/10.1016/j.agwat.2007.12.002

Konikow, L.F., 2011. The secret to successful solute-transport modeling. *Groundwater, 49*(2), 144–159. https://doi.org/10.1111/j.1745-6584.2010.00764.x

Lazareva, O., Druschel, G., & Pichler, T. (2015). Understanding arsenic behavior in carbonate aquifers: Implications for aquifer storage and recovery (ASR). *Applied Geochemistry, 52*, 57-66. https://doi.org/10.1016/j.apgeochem.2014.11.006

Lowry, C. S., & Anderson, M. P. (2006). An assessment of aquifer storage recovery using ground water flow models. *Groundwater, 44*(5), 661-667. https://doi.org/10.1111/j.1745-6584.2006.00237.x

Lu, C., Du, P., Chen, Y., & Luo, J. (2011). Recovery efficiency of aquifer storage and recovery (ASR) with mass transfer limitation. *Water Resources Research, 47*(8), 1–12. https://doi.org/10.1029/2011WR010605

Maliva, R. G., Guo, W., & Missimer, T. M. (2006). Aquifer storage and recovery: recent hydrogeological advances and system performance. *Water Environment Research, 78*(13), 2428-2435. https://doi.org/10.2175/106143006X123102

Maliva, R.G., and Missimer, T.M. (2010). *Aquifer storage and recovery and managed aquifer recharge using wells: Planning, hydrogeology, design, and operation.* Sugar Land, TX: Schlumberger.

Martin, R., 2013, Clogging Issues Associated with Managed Aquifer Recharge Methods. IAH Commission on Managing Aquifer Recharge, Australia, 213 p.

Miotlinski, K., Dillon, P. J., Pavelic, P., Barry, K., & Kremer, S. (2014). Recovery of injected freshwater from a brackish aquifer with a multiwell system. *Groundwater, 52*(4), 495-502. https://doi.org/10.1111/gwat.12089

Mirecki, J. E., Bennett, M. W., & López-Baláez, M. C. (2013). Arsenic control during aquifer storage recovery cycle tests in the floridan aquifer. *Groundwater, 51*(4), 539-549. https://doi.org/10.1111/j.1745-6584.2012.01001.x

Missimer, T. M., Drewes, J. E., Amy, G., Maliva, R. G., & Keller, S. (2012). Restoration of wadi aquifers by artificial recharge with treated waste water. *Ground Water, 50*(4), 514-527. https://doi.org/10.1111/j.1745-6584.2012.00941.x

Neil, C. W., Yang, Y. J., & Jun, Y. S. (2012). Arsenic mobilization and attenuation by mineral-water interactions: Implications for managed aquifer recharge. *Journal of Environmental Monitoring, 14*(7), 1772-1788. https://doi.org/10.1039/C2EM30323J

Neil, C. W., Jason Todd, M., & Jeffrey Yang, Y. (2018). Improving arsenopyrite oxidation rate laws: implications for arsenic mobilization during aquifer storage and recovery (ASR). *Environmental Geochemistry and Health, 2*, 1-12. 10.1007/s10653-018-0111-2

Pavelic, P., Dillon, P., & Robinson, N. (2004). Groundwater modelling to assist well-field design and operation for the ASTR trial at Salisbury, South Australia, Technical(27). https://doi.org/10.4225/08/586a96dcc0c14

Prommer, H., Sun, J., Helm, L., Rathi, B., Siade, A. J., & Morris, R. (2018). Deoxygenation Prevents Arsenic Mobilization during Deepwell Injection into Sulfide-Bearing Aquifers. *Environmental Science & Technology*, http://pubs.acs.org/doi/10.1021/acs.est.8b05015

Pyne, R. D. G., (2005). Aquifer Storage and Recovery: A Guide to Groundwater Recharge Through Wells, 2nd ed. ASR Systems LLC, Gainesville, Florida, USA.

Pyne, R. D. G. (2015). Aquifer storage recovery: an ASR solution to saltwater intrusion at Hilton Head Island, South Carolina, USA. *Environmental Earth Sciences, 73*(12), 7851-7859. https://doi.org/10.1007/s12665-014-3985-z

Schulze-Makuch, D. (2005). Longitudinal dispersivity data and implications for scaling behavior. *Groundwater 43*(3), 443–456. https://doi.org/10.1111/j.1745-6584.2005.0051.x

Sheng, Z. (2005). An aquifer storage and recovery system with reclaimed wastewater to preserve native groundwater resources in El Paso, Texas. *Journal of Environmental Management, 75*(4 SPEC. ISS.), 367–377. https://doi.org/10.1016/j.jenvman.2004.10.007

Smith, W. B., Miller, G. R., & Sheng, Z. (2017). Assessing aquifer storage and recovery feasibility in the Gulf Coastal Plains of Texas. *Journal of Hydrology: Regional Studies*, 14, 92–108. https://doi.org/10.1016/j.ejrh.2017.10.007

Vanderzalm, J. L., Page, D. W., Barry, K. E., & Dillon, P. J. (2010). A comparison of the geochemical response to different managed aquifer recharge operations for injection of urban stormwater in a carbonate aquifer. *Applied Geochemistry, 25*(9), 1350-1360. https://doi.org/10.1016/j.apgeochem.2010.06.005

Wallis, I., Prommer, H., Simmons, C. T., Post, V., & Stuyfzand, P. J. (2010). Evaluation of conceptual and numerical models for arsenic mobilization and attenuation during managed aquifer recharge. *Environmental Science and Technology*, *44*(13), 5035-5041. https://doi.org/10.1021/es100463q

Wallis, I., Prommer, H., Pichler, T., Post, V., & Simmons, C. (2011). Reactive Transport Modelling to Quantify Arsenic Mobilization and Capture during Aquifer Storage and Recovery of Potable Water. *Mineralogical Magazine, 75*(3), 2109-2109. https://doi.org/10.1021/es201286c

Wang, W., Lee, X., Xiao, W., Liu, S., Schultz, N., Wang, Y., et al. (2018). Global lake evaporation accelerated by changes in surface energy allocation in a warmer climate. *Nature Geoscience, 11*(6), 410-414. https://doi.org/10.1038/s41561-018-0114-8

Ward, J. D., Simmons, C. T., Dillon, P. J., & Pavelic, P. (2009). Integrated assessment of lateral flow, density effects and dispersion in aquifer storage and recovery. *Journal of Hydrology*, *370*(1–4), 83–99. https://doi.org/10.1016/j.jhydrol.2009.02.055

Webb, M. (2015). *Technical Note 15-04 Aquifer Storage and Recovery in Texas: 2015*. Retrieved from http://www.twdb.texas.gov/publications/reports/technical_notes/doc/TechnicalNote15-04.pdf

Williamson, M.A., Rimstidt, J.D., 1994. The kinetics and electrochemical rate determining step of aqueous pyrite oxidation. Geochim. Cosmochim. Acta 58 (24), 5443–5454. https://doi.org/10.1016/0016-7037(94)90241-0

Wurbs, R. A., & Ayala, R. A. (2014). Reservoir evaporation in Texas, USA. *Journal of Hydrology, 510*, 1-9. https://doi.org/10.1016/j.jhydrol.2013.12.011

Zhang, H., Gorelick, S. M., Zimba, P. V., & Zhang, X. (2017). A remote sensing method for estimating regional reservoir area and evaporative loss. *Journal of Hydrology, 555*, 213-227. https://doi.org/10.1016/j.jhydrol.2017.10.007

Zheng, C., Bennett, G.D., 2002. Applied Contaminant Transport Modeling. John Wiley and Sons Inc., New York.

Zuurbier, K. G., Bakker, M., Zaadnoordijk, W. J., & Stuyfzand, P. J. (2013). Identification of potential sites for aquifer storage and recovery (ASR) in coastal areas using ASR performance estimation methods. *Hydrogeology Journal, 21*(6), 1373-1383. https://doi.org/10.1007/s10040-013-1003-2

Zuurbier, K. G., Hartog, N., & Stuyfzand, P. J. (2016). Reactive transport impacts on recovered freshwater quality during multiple partially penetrating wells (MPPW) ASR in a brackish heterogeneous aquifer. *Applied Geochemistry, 71*, 35-47. https://doi.org/10.1016/j.apgeochem.2016.05.013

APPENDIX A

MODIFIED PHC PACKAGE FOR FLOPY

```
from ..pakbase import Package


class Mt3dPhc(Package):
    """
    PHC package class for PHT3D
    """
    unitnumber = 38

    def __init__(self, model, os=2, temp=25, asbin=0, eps_aqu=0, eps_ph=0,
                 scr_output=1, cb_offset=0, smse=['pH', 'pe'], mine=[], ie=[],
                 surf=[], mobkin=[], minkin=[], surfkin=[], imobkin=[],
                 extension='phc', unitnumber=None, filenames=None):

        if unitnumber is None:
            unitnumber = Mt3dPhc.defaultunit()
        elif unitnumber == 0:
            unitnumber = Mt3dPhc.reservedunit()

        # set filenames
        if filenames is None:
            filenames = [None]
        elif isinstance(filenames, str):
            filenames = [filenames]

        # Fill namefile items
        name = [Mt3dPhc.ftype()]
        units = [unitnumber]
        extra = ['']

        # set package name
        fname = [filenames[0]]

        # Call ancestor's init to set self.parent, extension, name and unit number
        Package.__init__(self, model, extension=extension, name=name,
                         unit_number=units, extra=extra, filenames=fname)

        self.os = os
        self.temp = temp
        self.asbin = asbin
        self.eps_aqu = eps_aqu
```

```
    self.eps_ph = eps_ph
    self.scr_output = scr_output
    self.cb_offset = cb_offset
    self.smse = smse
    self.nsmse = len(self.smse)
    self.mine = mine
    self.nmine = len(self.mine)
    self.ie = ie
    self.nie = len(self.ie)
    self.surf = surf
    self.nsurf = len(self.surf)
    self.surf_parms = surf[1]
    self.mobkin = mobkin
    self.nmobkin = len(self.mobkin)
    self.minkin = minkin[0]
    self.nminkin = len(self.minkin)
    self.minkin_parms = minkin[1]
    self.surfkin = surfkin
    self.nsurfkin = len(self.surfkin)
    self.imobkin = imobkin
    self.nimobkin = len(self.imobkin)
    self.parent.add_package(self)
    return

def __repr__(self):
    return 'PHC package class for PHT3D'

def write_file(self):
    """
    Write the package file

    Returns
    -------
    None

    """
    # Open file for writing
    f_phc = open(self.fn_path, 'w')
    f_phc.write('%.0d %.1f %.0d %.10f %.10f %.0d\n' % (self.os, self.temp,
                                    self.asbin, self.eps_aqu,
                                    self.eps_ph, self.scr_output))
    f_phc.write('%.1f\n' % (self.cb_offset))
    f_phc.write('%.0d\n' % (self.nsmse))
    f_phc.write('%.0d\n' % (self.nmine))
    f_phc.write('%.0d\n' % (self.nie))
```

```
    f_phc.write('%.0d\n' % (self.nsurf))
    f_phc.write('%.0d%2.0d%2.0d%2.0d\n' % (self.nmobkin, self.nminkin,
                                self.nsurfkin, self.nimobkin))
    for s in self.smse:
        f_phc.write('%s\n' % (s))
    for e in self.mine:
        f_phc.write('%s\n' % (e))
    for ie in self.ie:
        f_phc.write('%s\n' % (ie))
    for surf in self.surf:
        f_phc.write('%s\n' % (surf))
    f_phc.write('\n')
    i = 0
    for m in self.minkin:
        f_phc.write('%s %d\n' % (m, len(self.minkin_parms)))
        for n in self.minkin_parms:
            f_phc.write('%.10f\n' % (n))
    f_phc.close()

    return

@staticmethod
def ftype():
    return 'PHC'

@staticmethod
def defaultunit():
    return 38

@staticmethod
def reservedunit():
    return 38
```

APPENDIX B

ADDITIONS TO WATEQ4F DATABASE

Additions to the WATEQ4F database are given below. These must be inserted into the relevant data block (e.g., PHASES).

PHASES

```
As-Pyrite       #Antoniou et al. (2015)
      FeAs0.008S1.992 + 1.968H+ + 0.024H2O +  1.96e- = Fe+2 + 0.008H3AsO3 + 1.992HS-
      log_k          -18.479
      delta_h 11.3 kcal
```

RATES

```
As-Pyrite
  -start
  1 rem parm(1) = log10(A/V, 1/dm)  parm(2) = exp for (m/m0)
  2 rem parm(3) = exp for O2              parm(4) = exp for H+

  10 if (m <= 0) then goto 200
  20 if (si("Pyrite") >= 0) then goto 200
  20  rate = -10.19 + parm(1) + parm(3)*lm("O2") + parm(4)*lm("H+") + parm(2)*log10(m/m0)
  30  moles = 10^rate * time
  40 if (moles > m) then moles = m
  50 if (moles >= (mol("O2")/3.5)) then moles = mol("O2")/3.5
  200 save moles
  -end
```

APPENDIX C

PHT3D INTERFACE FILE

```
2 13.0 1 0.0000000001 0.0010000000 1
0.0
15
2
5
2
0 1 0 0
As
C(4)
C(-4)
Ca
Cl
Fe(2)
Fe(3)
K
Mg
Na
O(0)
S(-2)
S(6)
pH
pe
Calcite
Fe(OH)3(a)
CaX2
MgX2
NaX
KX
FeX2
Hfo_sOH 0.0 0.0 Fe(OH)3(a) equilibrium_phase
Hfo_wOH 53300.0 0.0 Fe(OH)3(a) equilibrium_phase

As-Pyrite 4
1.6500000000
0.6700000000
0.5000000000
-0.1100000000
```

APPENDIX D

CUMULATIVE REN'S AND MIXING FRACTIONS

Table D-1. Mixing Fraction at the end of simulation and cumulative REN for all hydraulic gradients with zero-day storage.

Hydraulic Gradient	Pumping Scenario	Mixing Fraction at the end of simulation	Cumulative REN (%)
0.0001	Slow Extraction	0.725	84.81
	Slow Injection	0.725	84.85
	Baseline	0.726	84.87
	Fast Injection	0.727	84.92
	Fast Extraction	0.727	85.04
0.001	Slow Extraction	0.668	83.22
	Slow Injection	0.670	83.28
	Baseline	0.689	83.86
	Fast Injection	0.706	84.38
	Fast Extraction	0.707	84.52
0.0025	Slow Extraction	0.508	77.32
	Slow Injection	0.515	77.39
	Baseline	0.566	79.71
	Fast Injection	0.623	81.93
	Fast Extraction	0.628	82.11
0.005	Slow Extraction	0.323	66.28
	Slow Injection	0.343	66.36
	Baseline	0.398	71.11
	Fast Injection	0.475	76.02
	Fast Extraction	0.490	76.27

Table D-2. Mixing Fraction at the end of simulation and cumulative REN for all hydraulic gradients with six-month storage.

Hydraulic Gradient	Pumping Scenario	Mixing Fraction at the end of simulation	Cumulative REN (%)
0.0001	Slow Extraction	0.725	84.77
	Slow Injection	0.725	84.81
	Baseline	0.726	84.84
	Fast Injection	0.727	84.88
	Fast Extraction	0.727	85.02
0.001	Slow Extraction	0.585	78.79
	Slow Injection	0.589	78.85
	Baseline	0.610	79.77
	Fast Injection	0.632	80.70
	Fast Extraction	0.634	80.86
0.0025	Slow Extraction	0.381	63.46
	Slow Injection	0.396	63.54
	Baseline	0.420	66.11
	Fast Injection	0.453	68.78
	Fast Extraction	0.466	69.04
0.005	Slow Extraction	0.142	34.69
	Slow Injection	0.162	34.07
	Baseline	0.186	39.22
	Fast Injection	0.217	44.77
	Fast Extraction	0.252	45.18

Table D-3. Mixing Fraction at the end of simulation and cumulative REN for all hydraulic gradients with one-year storage.

Hydraulic Gradient	Pumping Scenario	Mixing Fraction at the end of simulation	Cumulative REN (%)
0.0001	Slow Extraction	0.722	84.68
	Slow Injection	0.723	84.73
	Baseline	0.724	84.76
	Fast Injection	0.725	84.81
	Fast Extraction	0.725	84.94
0.001	Slow Extraction	0.516	73.59
	Slow Injection	0.521	73.68
	Baseline	0.538	74.70
	Fast Injection	0.558	75.81
	Fast Extraction	0.561	75.96
0.0025	Slow Extraction	0.308	50.05
	Slow Injection	0.327	50.12
	Baseline	0.342	52.59
	Fast Injection	0.360	55.21
	Fast Extraction	0.378	55.40
0.005	Slow Extraction	0.119	18.20
	Slow Injection	0.145	18.21
	Baseline	0.162	21.47
	Fast Injection	0.181	25.28
	Fast Extraction	0.214	25.15

APPENDIX E

CUMULATIVE NON-SORBED ARSENIC VS. TIME

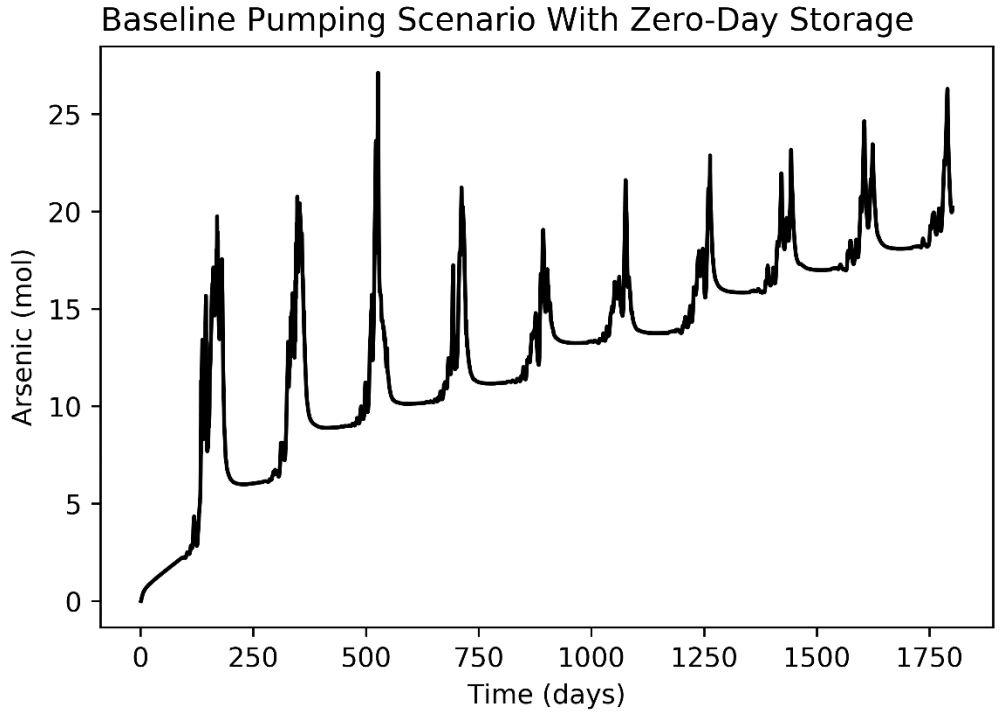

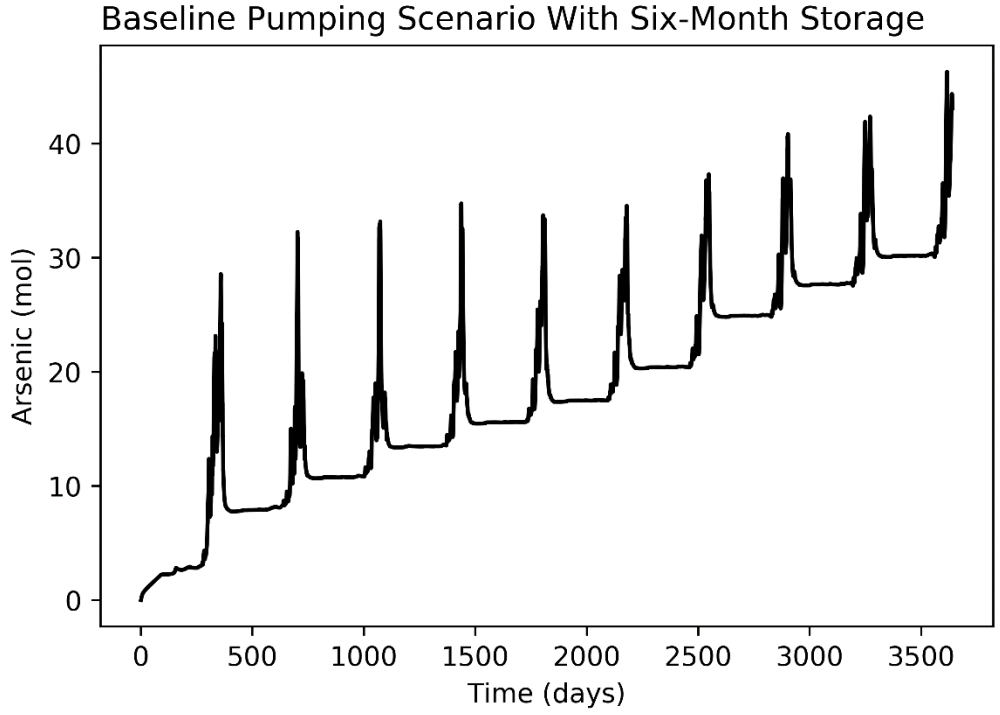

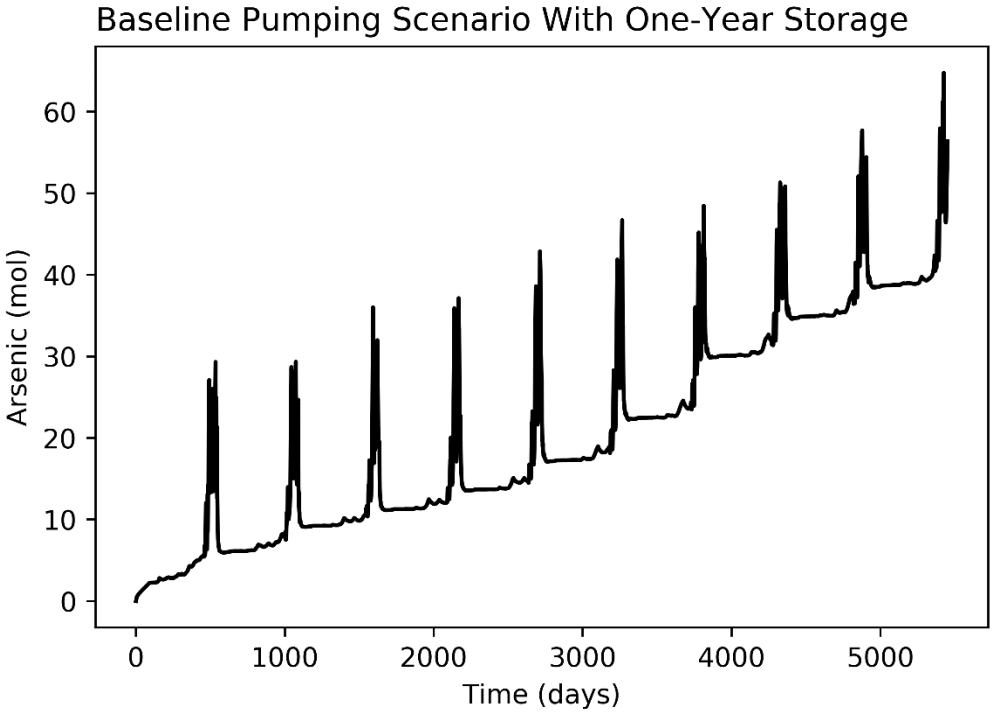
Baseline Pumping Scenario With One-Year Storage
Arsenic (mol)
0
10
20
30
40
50
60
0
1000
2000
3000
4000
5000
Time (days)

APPENDIX F

ARSENIC CONCENTRATIONS VS. TIME AT THE WELL

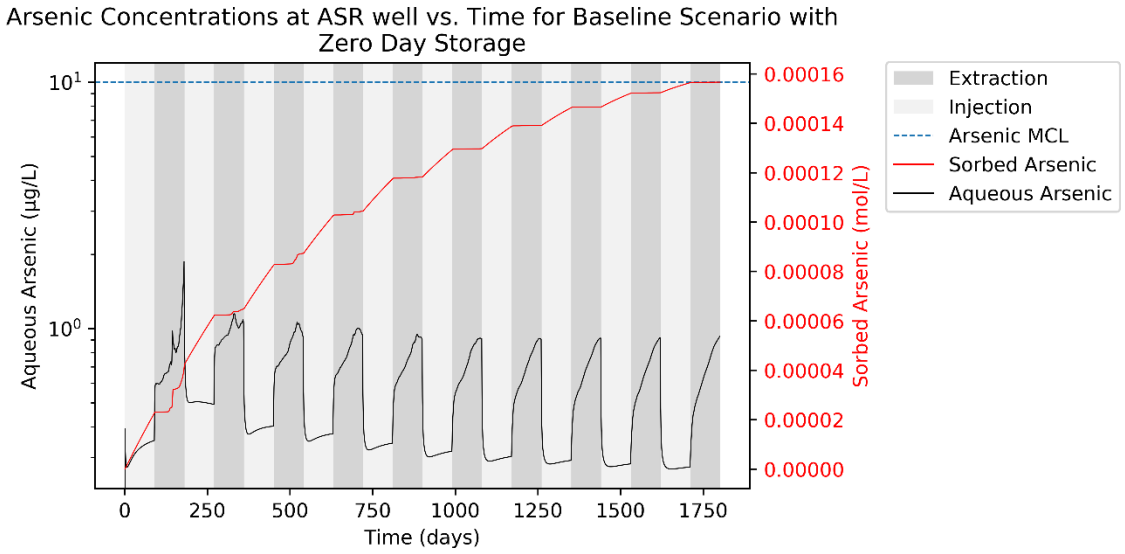

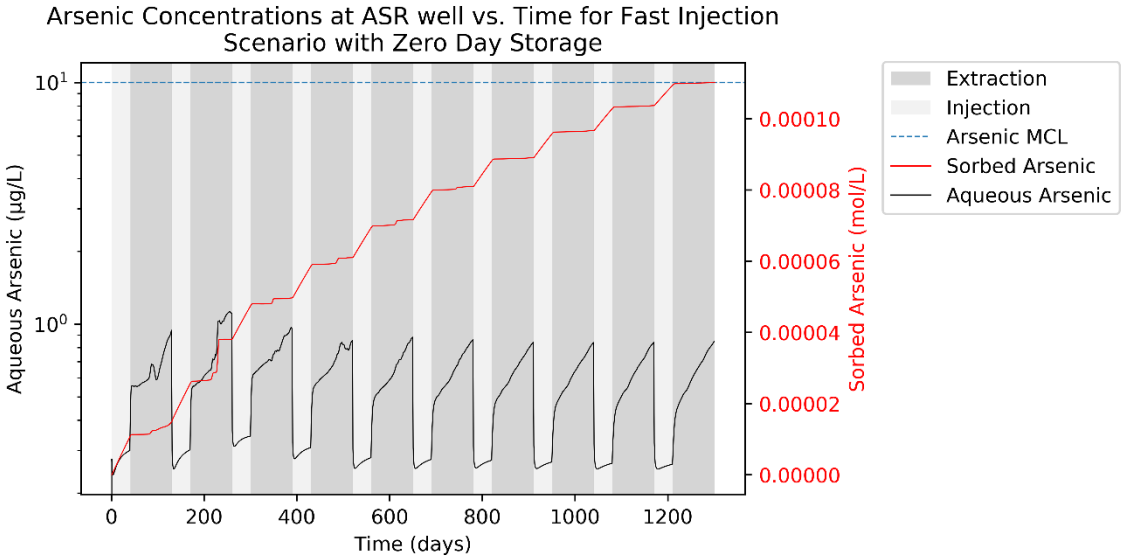

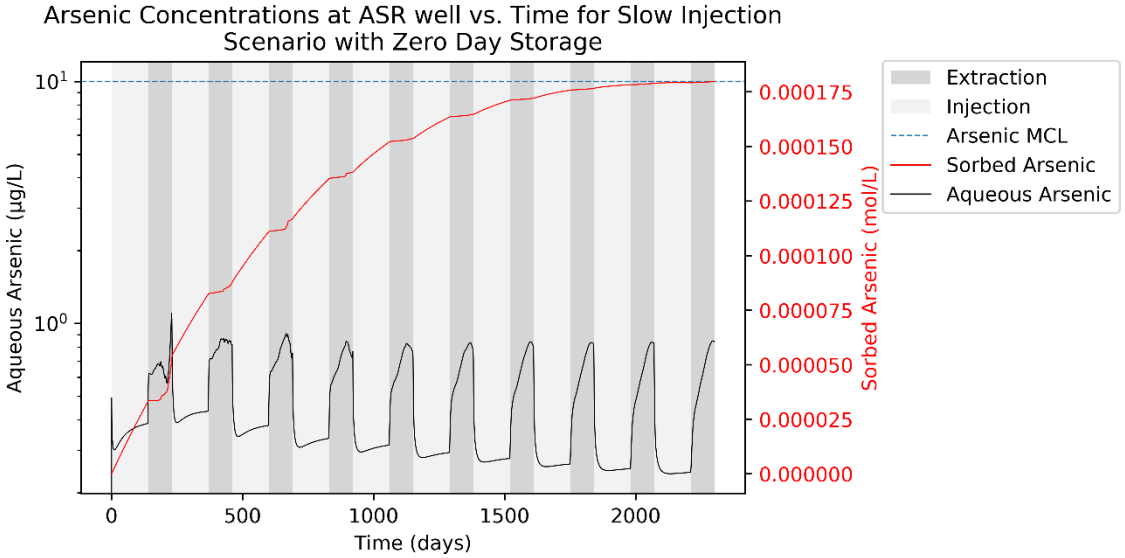
Arsenic Concentrations at ASR well vs. Time for Slow Injection Scenario with Zero Day Storage
Aqueous Arsenic (µg/L)
Sorbed Arsenic (mol/L)
Time (days)
Extraction
Injection
Arsenic MCL
Sorbed Arsenic
Aqueous Arsenic

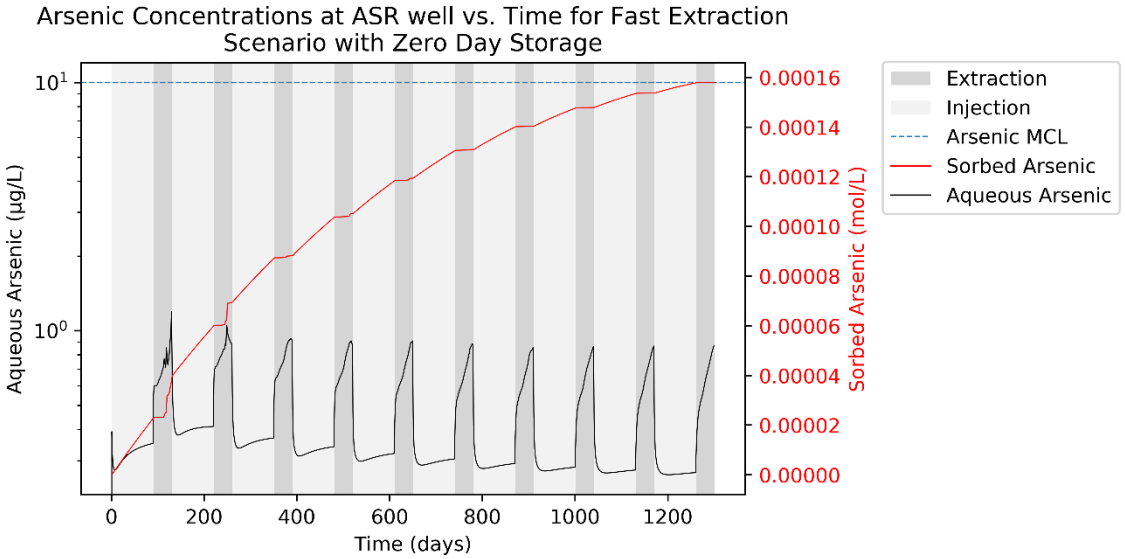
Arsenic Concentrations at ASR well vs. Time for Fast Extraction Scenario with Zero Day Storage
Aqueous Arsenic (µg/L)
Sorbed Arsenic (mol/L)
Time (days)
Extraction
Injection
Arsenic MCL
Sorbed Arsenic
Aqueous Arsenic

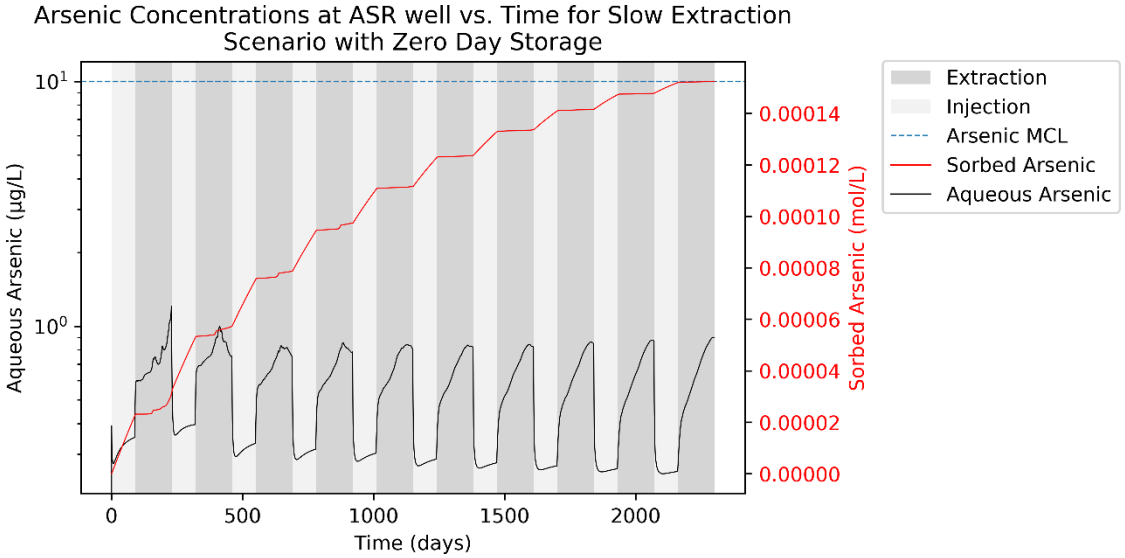
Arsenic Concentrations at ASR well vs. Time for Slow Extraction Scenario with Zero Day Storage
Aqueous Arsenic (µg/L)
Sorbed Arsenic (mol/L)
Time (days)
Extraction
Injection
Arsenic MCL
Sorbed Arsenic
Aqueous Arsenic

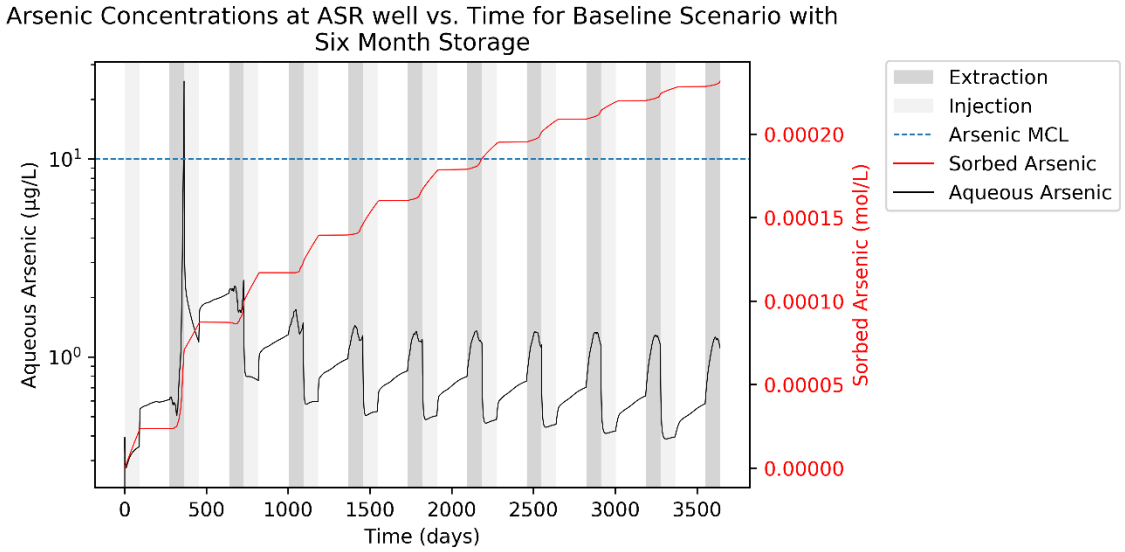
Arsenic Concentrations at ASR well vs. Time for Baseline Scenario with Six Month Storage
Aqueous Arsenic (µg/L)
Sorbed Arsenic (mol/L)
Time (days)
Extraction
Injection
Arsenic MCL
Sorbed Arsenic
Aqueous Arsenic

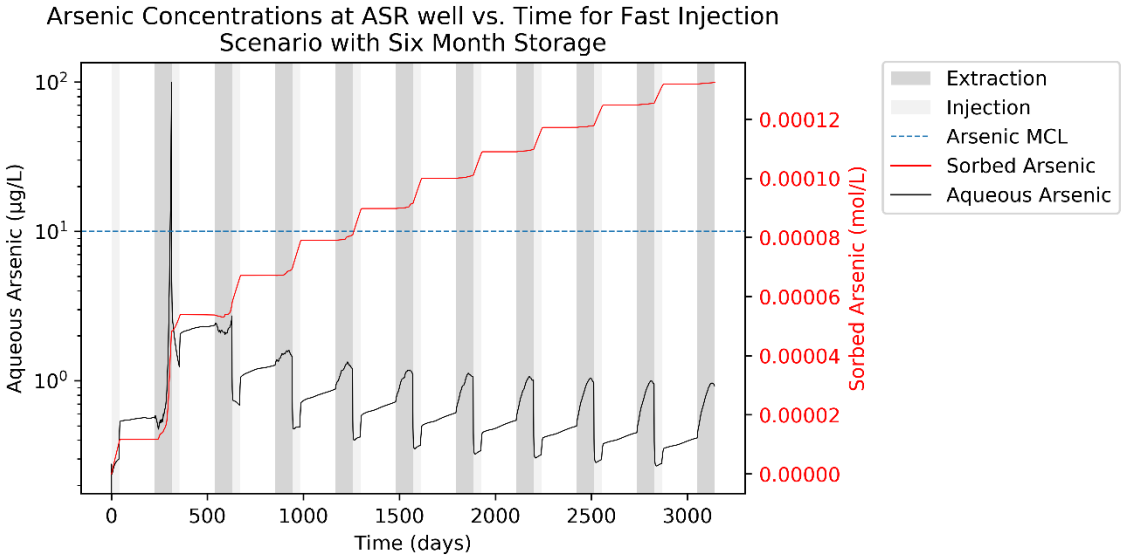
Arsenic Concentrations at ASR well vs. Time for Fast Injection Scenario with Six Month Storage
Aqueous Arsenic (µg/L)
Sorbed Arsenic (mol/L)
Time (days)
Extraction
Injection
Arsenic MCL
Sorbed Arsenic
Aqueous Arsenic

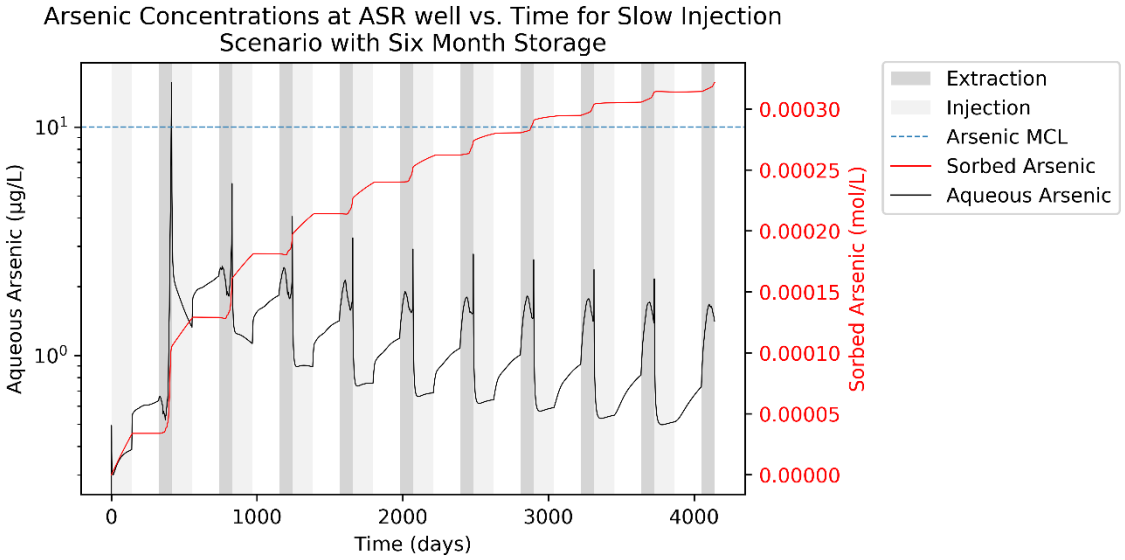
Arsenic Concentrations at ASR well vs. Time for Slow Injection Scenario with Six Month Storage
Aqueous Arsenic (µg/L)
Sorbed Arsenic (mol/L)
Time (days)
Extraction
Injection
Arsenic MCL
Sorbed Arsenic
Aqueous Arsenic

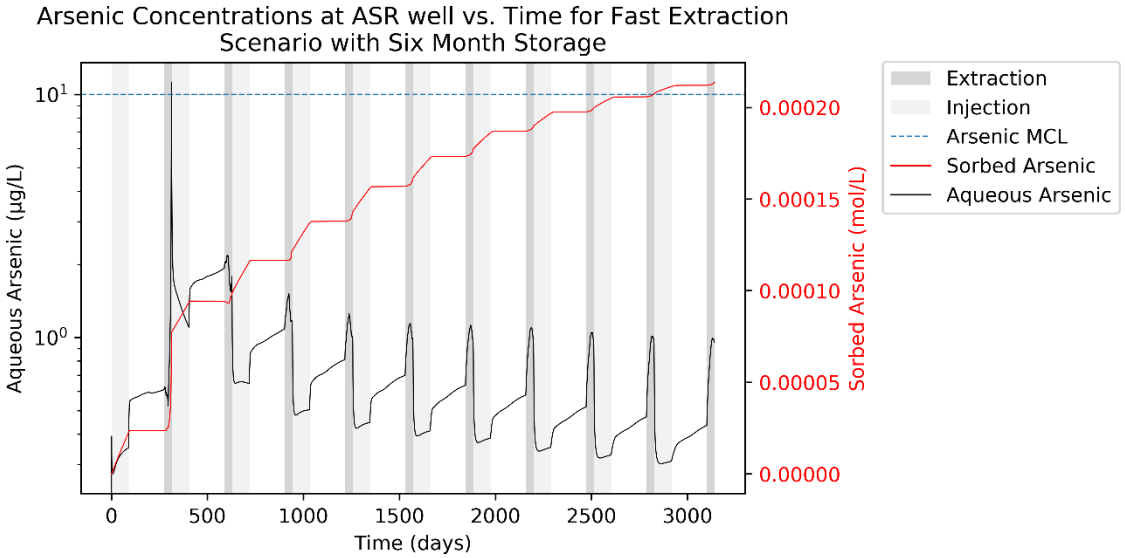
Arsenic Concentrations at ASR well vs. Time for Fast Extraction Scenario with Six Month Storage
Aqueous Arsenic (µg/L)
Sorbed Arsenic (mol/L)
Time (days)
Extraction
Injection
Arsenic MCL
Sorbed Arsenic
Aqueous Arsenic

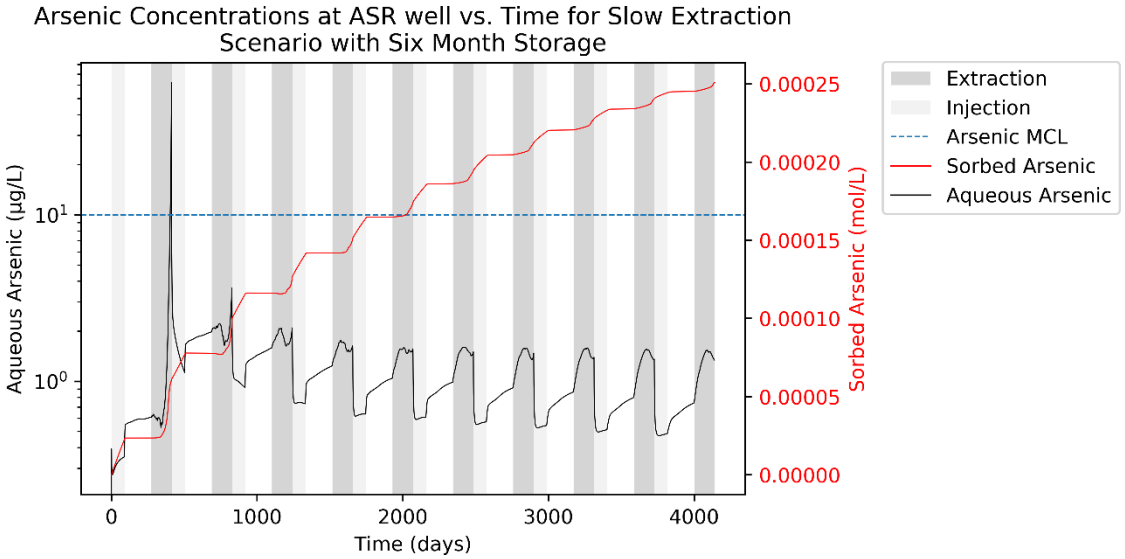
Arsenic Concentrations at ASR well vs. Time for Slow Extraction Scenario with Six Month Storage
Aqueous Arsenic (µg/L)
Sorbed Arsenic (mol/L)
Time (days)
Extraction
Injection
Arsenic MCL
Sorbed Arsenic
Aqueous Arsenic

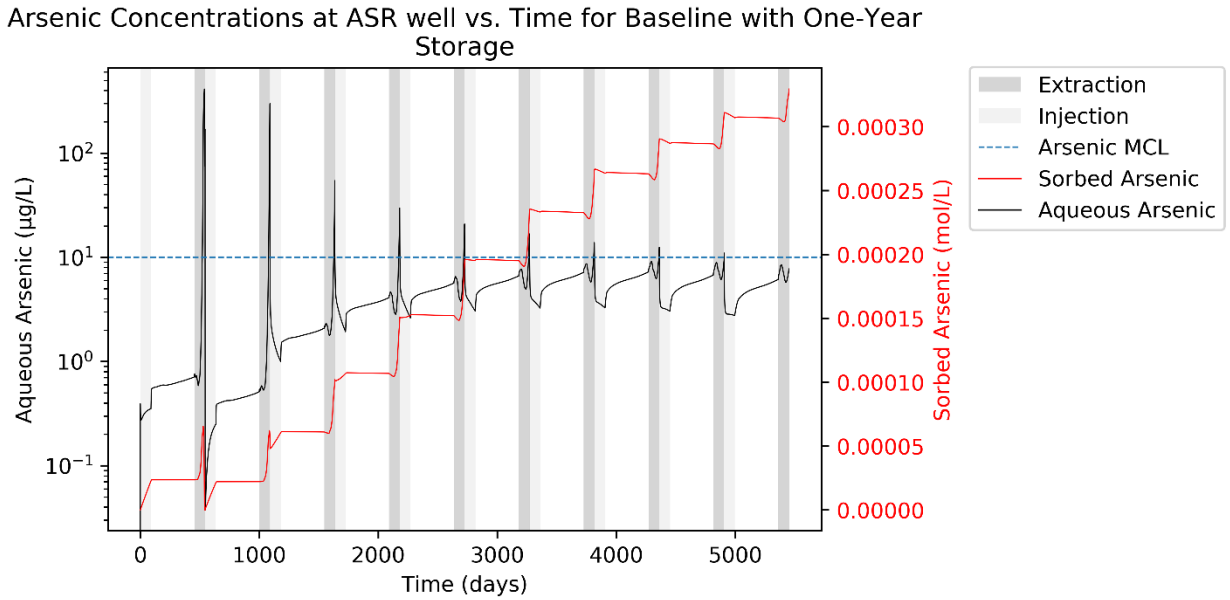
Arsenic Concentrations at ASR well vs. Time for Baseline with One-Year Storage
Aqueous Arsenic (µg/L)
Sorbed Arsenic (mol/L)
Time (days)
Extraction
Injection
Arsenic MCL
Sorbed Arsenic
Aqueous Arsenic

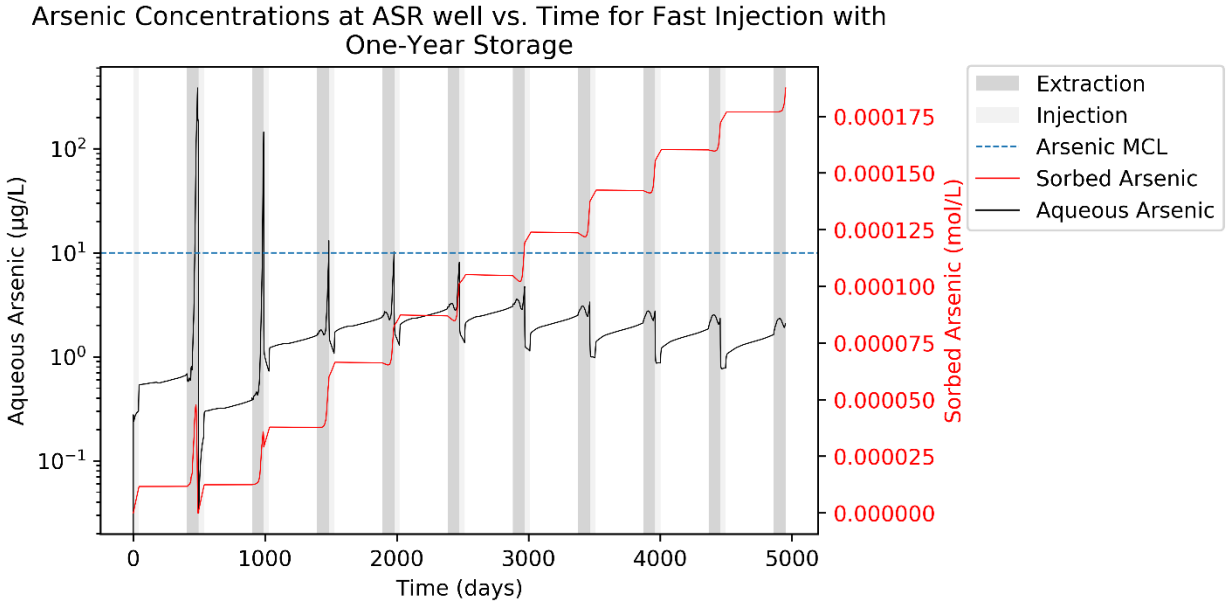
Arsenic Concentrations at ASR well vs. Time for Fast Injection with One-Year Storage
Aqueous Arsenic (µg/L)
Sorbed Arsenic (mol/L)
Time (days)
Extraction
Injection
Arsenic MCL
Sorbed Arsenic
Aqueous Arsenic

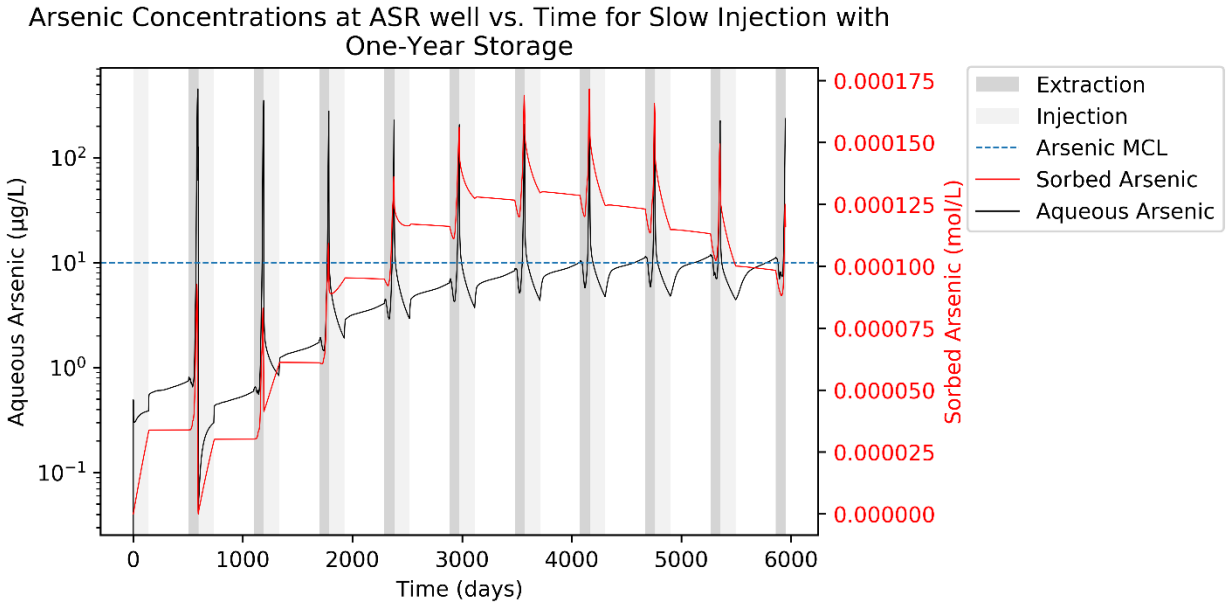
Arsenic Concentrations at ASR well vs. Time for Slow Injection with One-Year Storage
Aqueous Arsenic (µg/L)
Sorbed Arsenic (mol/L)
Time (days)
Extraction
Injection
Arsenic MCL
Sorbed Arsenic
Aqueous Arsenic

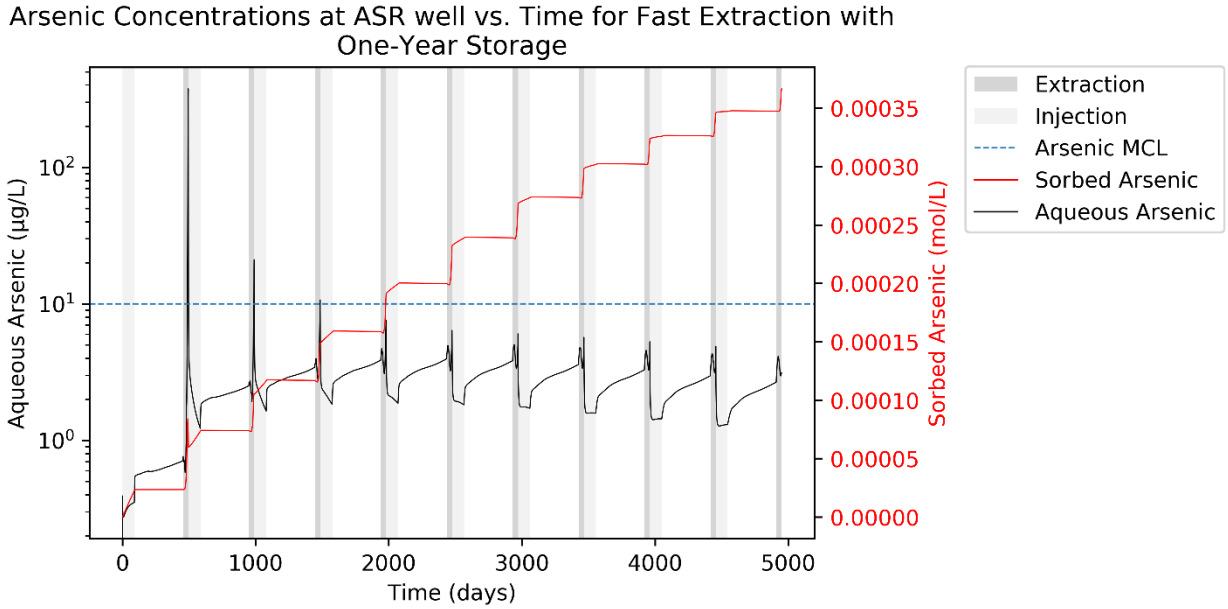
Arsenic Concentrations at ASR well vs. Time for Fast Extraction with One-Year Storage
Aqueous Arsenic (µg/L)
Sorbed Arsenic (mol/L)
Time (days)
Extraction
Injection
Arsenic MCL
Sorbed Arsenic
Aqueous Arsenic

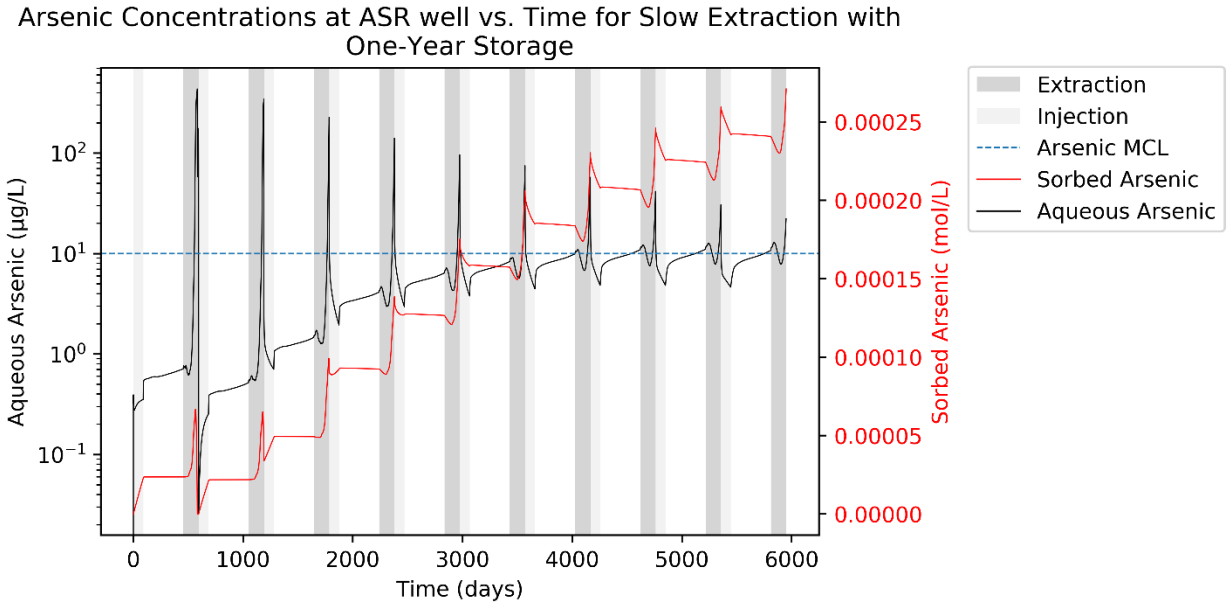
Arsenic Concentrations at ASR well vs. Time for Slow Extraction with One-Year Storage
Aqueous Arsenic (µg/L)
Sorbed Arsenic (mol/L)
Time (days)
Extraction
Injection
Arsenic MCL
Sorbed Arsenic
Aqueous Arsenic

APPENDIX G

HFO CONCENTRATIONS VS. TIME AT THE WELL

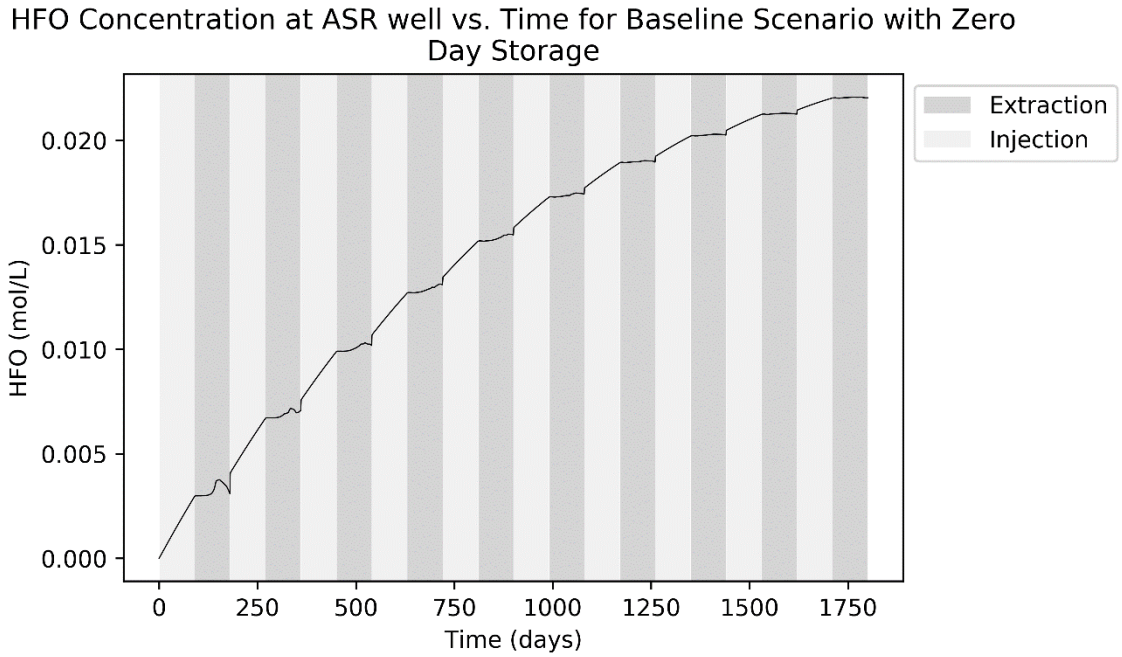

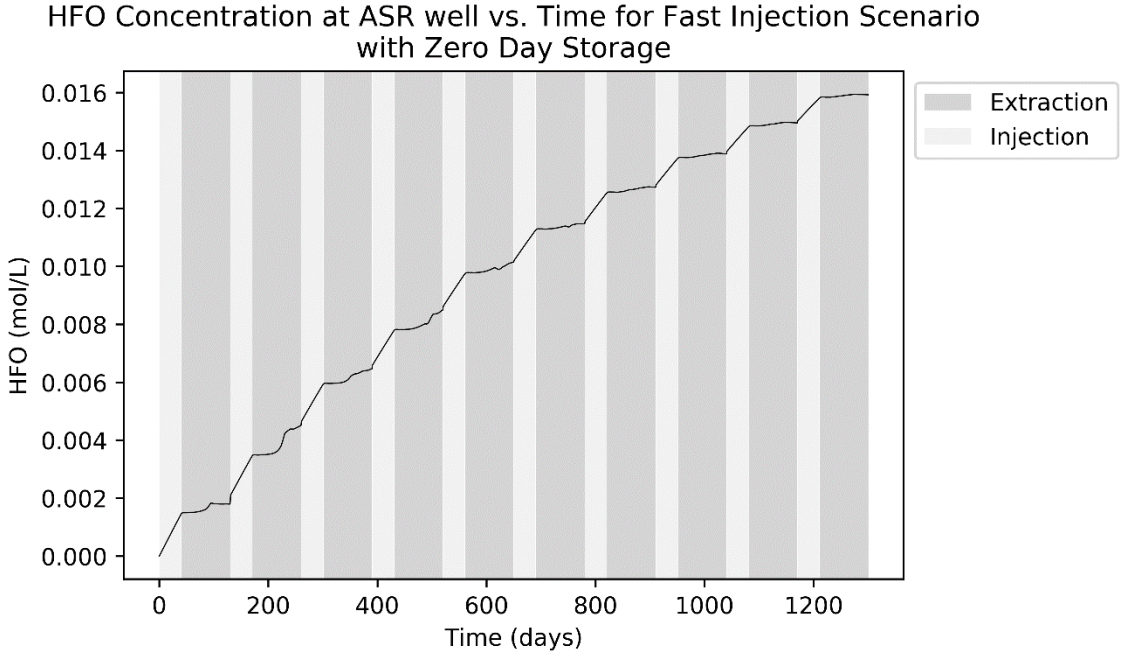

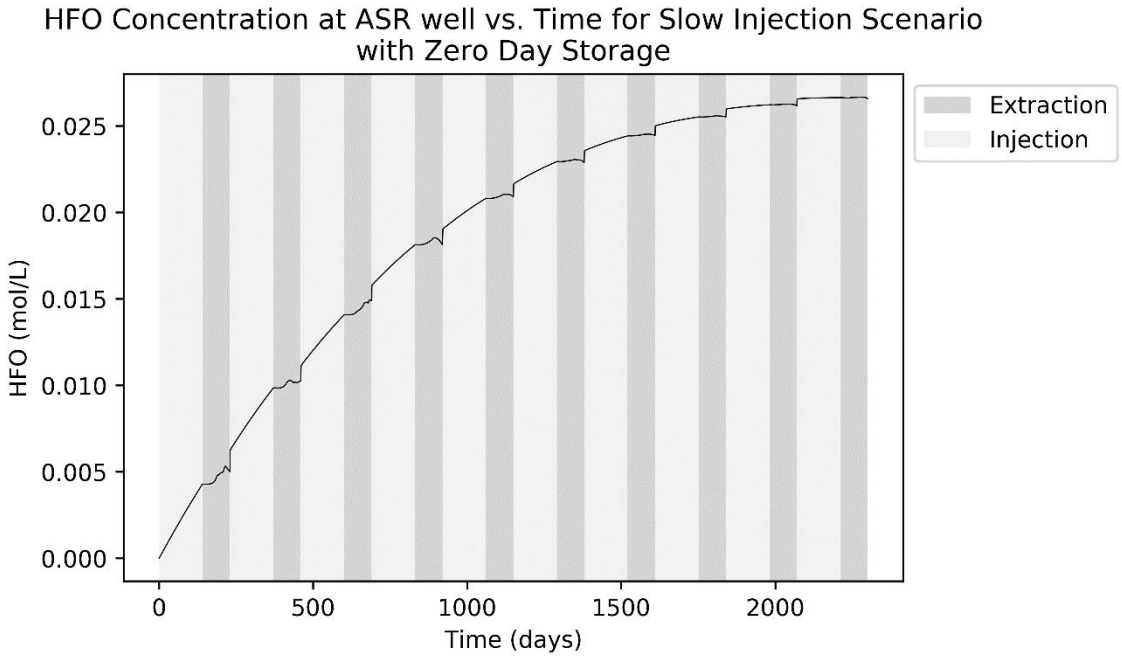
HFO Concentration at ASR well vs. Time for Slow Injection Scenario
with Zero Day Storage
HFO (mol/L)
0.000
0.005
0.010
0.015
0.020
0.025
0
500
1000
1500
2000
Time (days)
Extraction
Injection

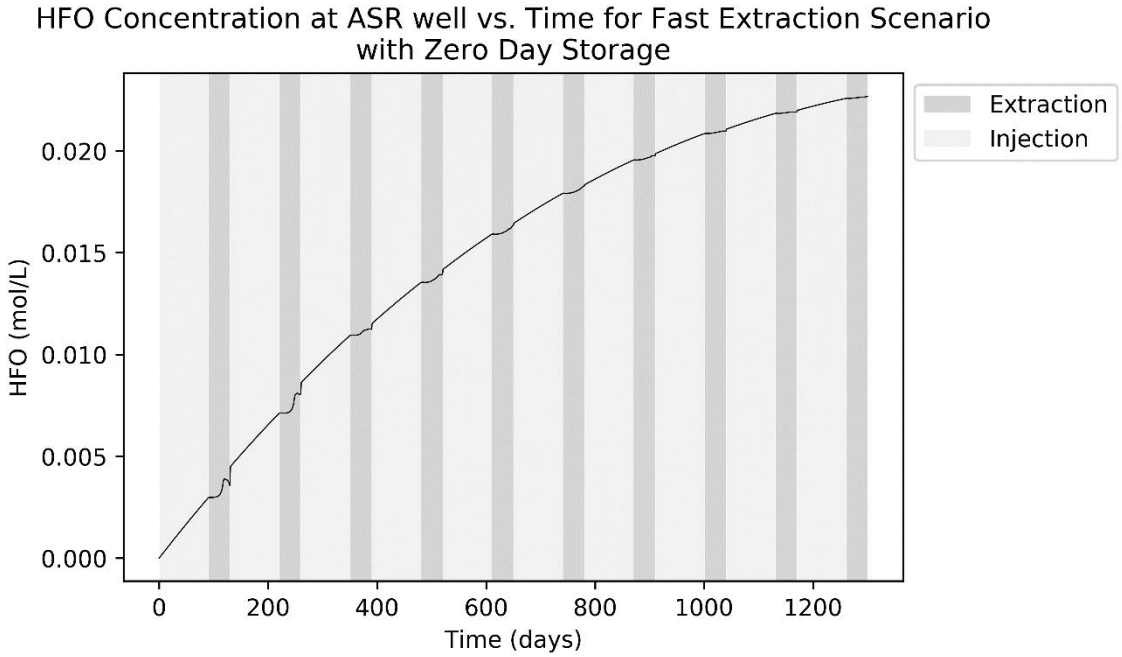
HFO Concentration at ASR well vs. Time for Fast Extraction Scenario
with Zero Day Storage
HFO (mol/L)
0.000
0.005
0.010
0.015
0.020
0
200
400
600
800
1000
1200
Time (days)
Extraction
Injection

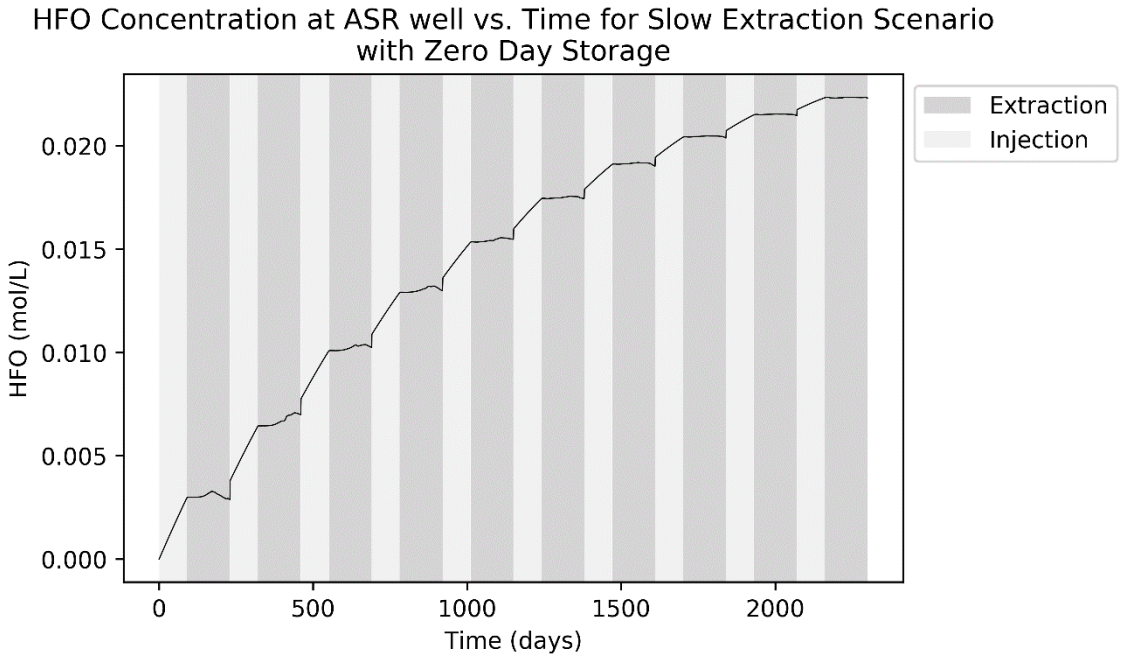
HFO Concentration at ASR well vs. Time for Slow Extraction Scenario with Zero Day Storage
HFO (mol/L)
0.000
0.005
0.010
0.015
0.020
0
500
1000
1500
2000
Time (days)
Extraction
Injection

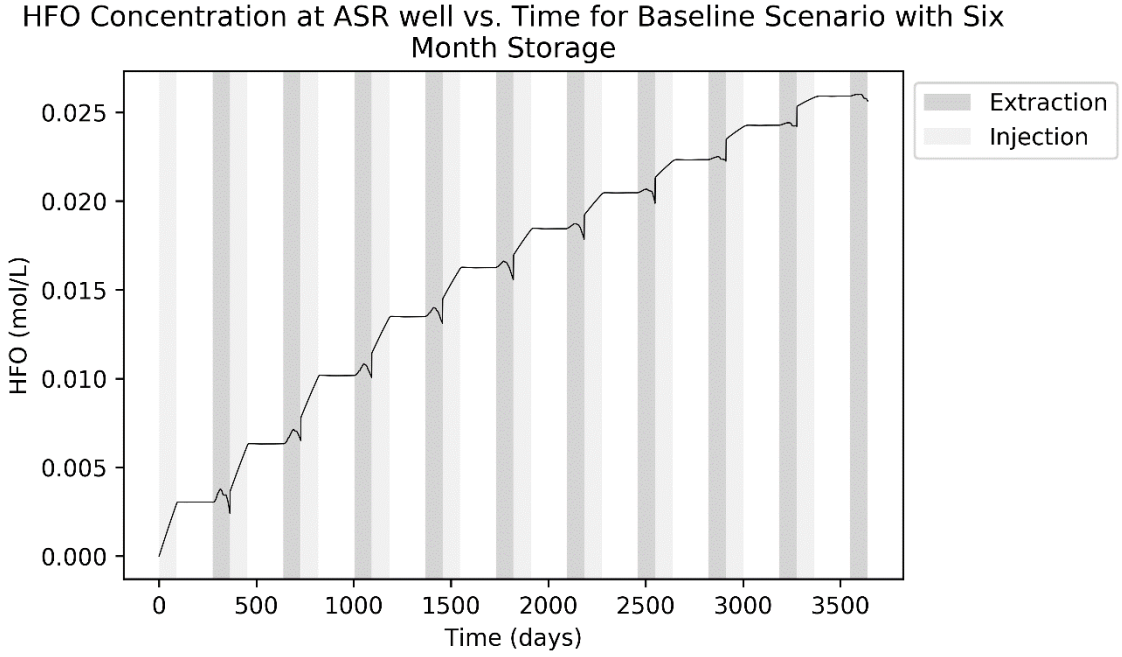
HFO Concentration at ASR well vs. Time for Baseline Scenario with Six Month Storage
HFO (mol/L)
0.000
0.005
0.010
0.015
0.020
0.025
0
500
1000
1500
2000
2500
3000
3500
Time (days)
Extraction
Injection

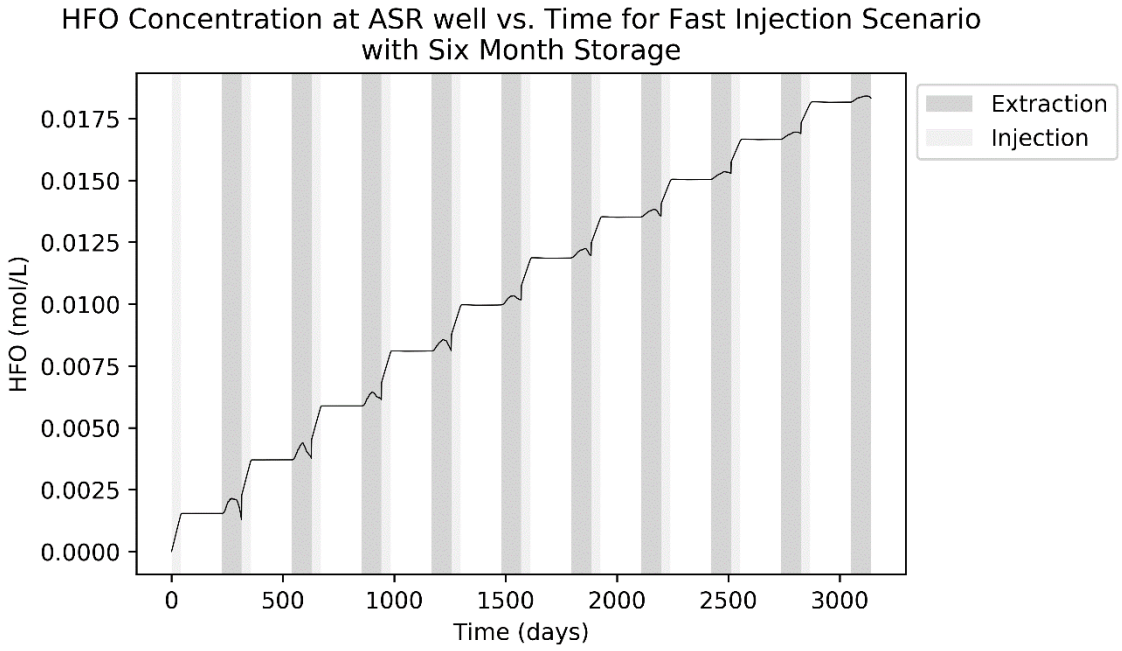
HFO Concentration at ASR well vs. Time for Fast Injection Scenario
with Six Month Storage
HFO (mol/L)
0.0175
0.0150
0.0125
0.0100
0.0075
0.0050
0.0025
0.0000
0
500
1000
1500
2000
2500
3000
Time (days)
Extraction
Injection

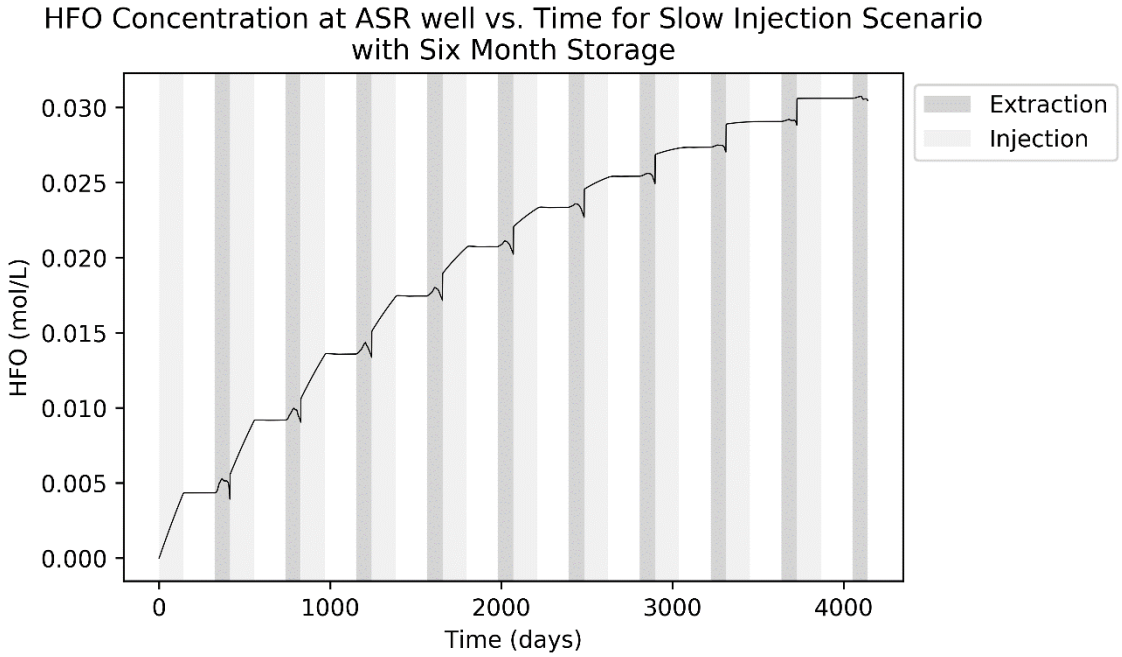
HFO Concentration at ASR well vs. Time for Slow Injection Scenario
with Six Month Storage
HFO (mol/L)
0.030
0.025
0.020
0.015
0.010
0.005
0.000
0
1000
2000
3000
4000
Time (days)
Extraction
Injection

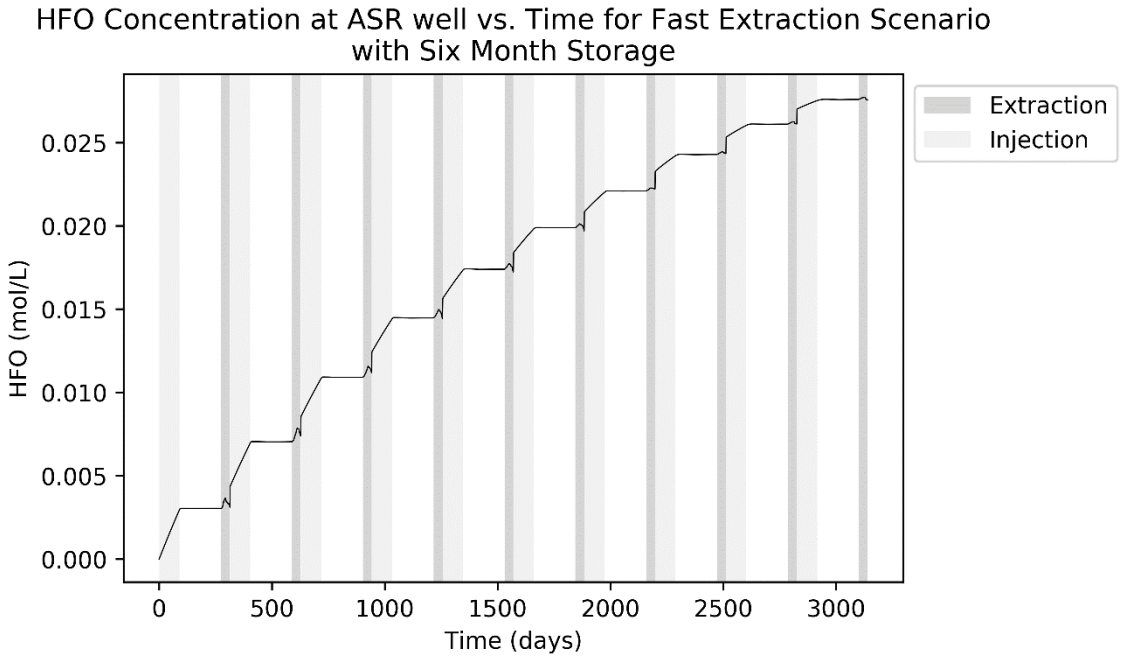
HFO Concentration at ASR well vs. Time for Fast Extraction Scenario
with Six Month Storage
Extraction
Injection
HFO (mol/L)
0.000
0.005
0.010
0.015
0.020
0.025
0
500
1000
1500
2000
2500
3000
Time (days)

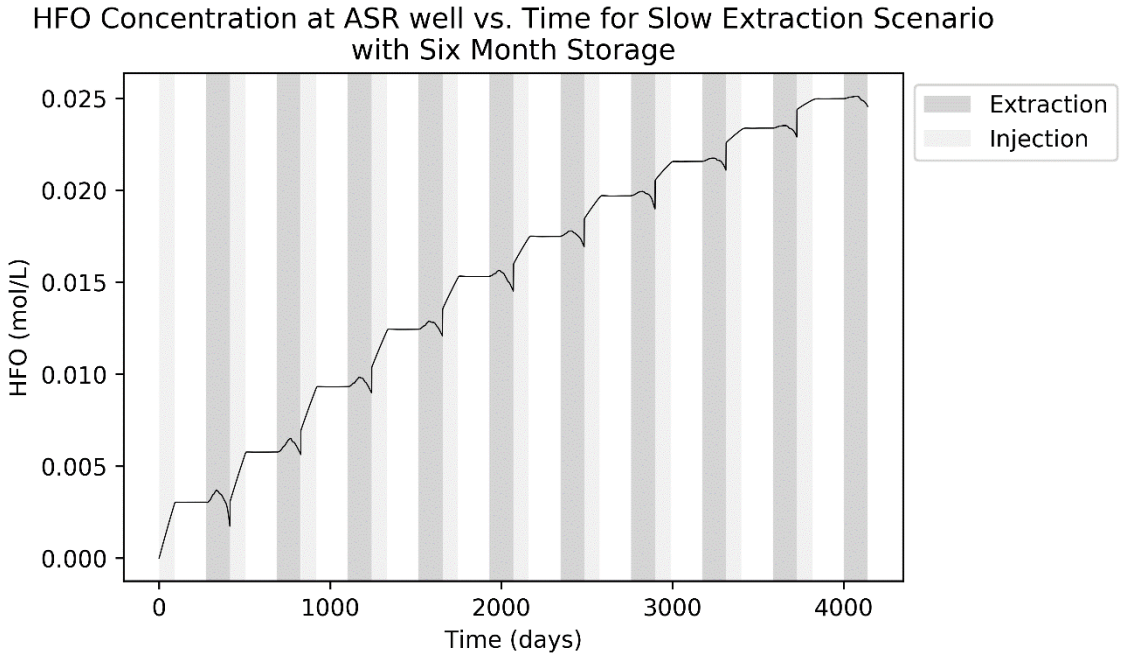
HFO Concentration at ASR well vs. Time for Slow Extraction Scenario
with Six Month Storage
Extraction
Injection
HFO (mol/L)
0.000
0.005
0.010
0.015
0.020
0.025
0
1000
2000
3000
4000
Time (days)

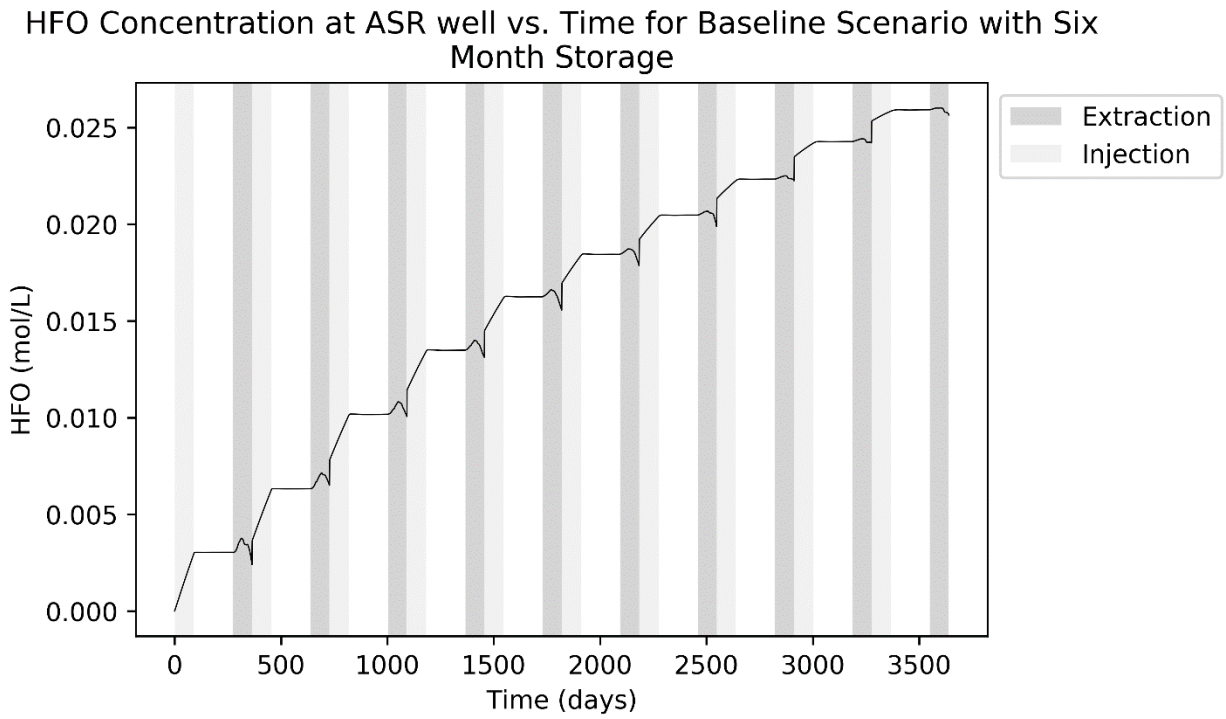
HFO Concentration at ASR well vs. Time for Baseline Scenario with Six Month Storage
HFO (mol/L)
0.000
0.005
0.010
0.015
0.020
0.025
0
500
1000
1500
2000
2500
3000
3500
Time (days)
Extraction
Injection

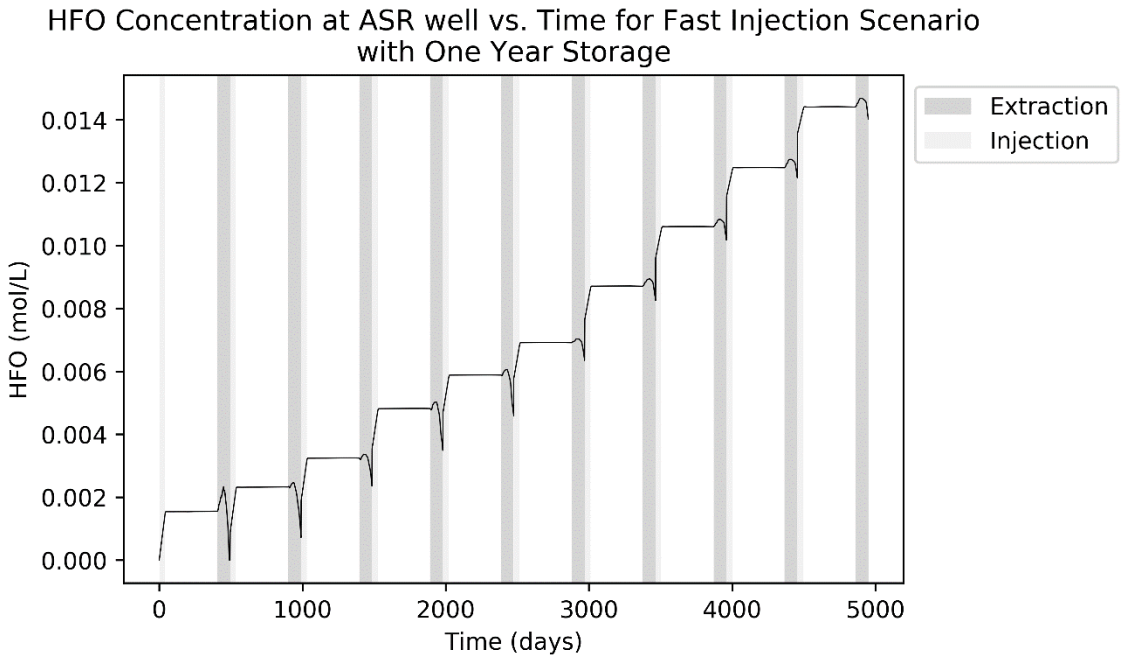
HFO Concentration at ASR well vs. Time for Fast Injection Scenario with One Year Storage
HFO (mol/L)
0.000
0.002
0.004
0.006
0.008
0.010
0.012
0.014
0
1000
2000
3000
4000
5000
Time (days)
Extraction
Injection

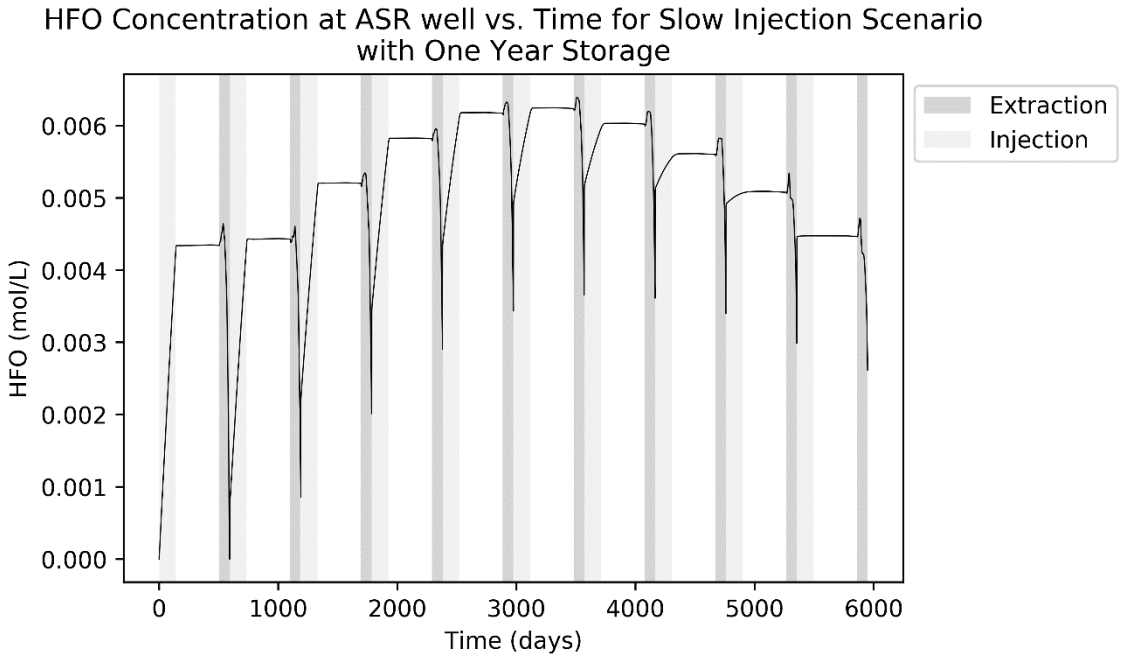
HFO Concentration at ASR well vs. Time for Slow Injection Scenario
with One Year Storage
HFO (mol/L)
0.000
0.001
0.002
0.003
0.004
0.005
0.006
0
1000
2000
3000
4000
5000
6000
Time (days)
Extraction
Injection

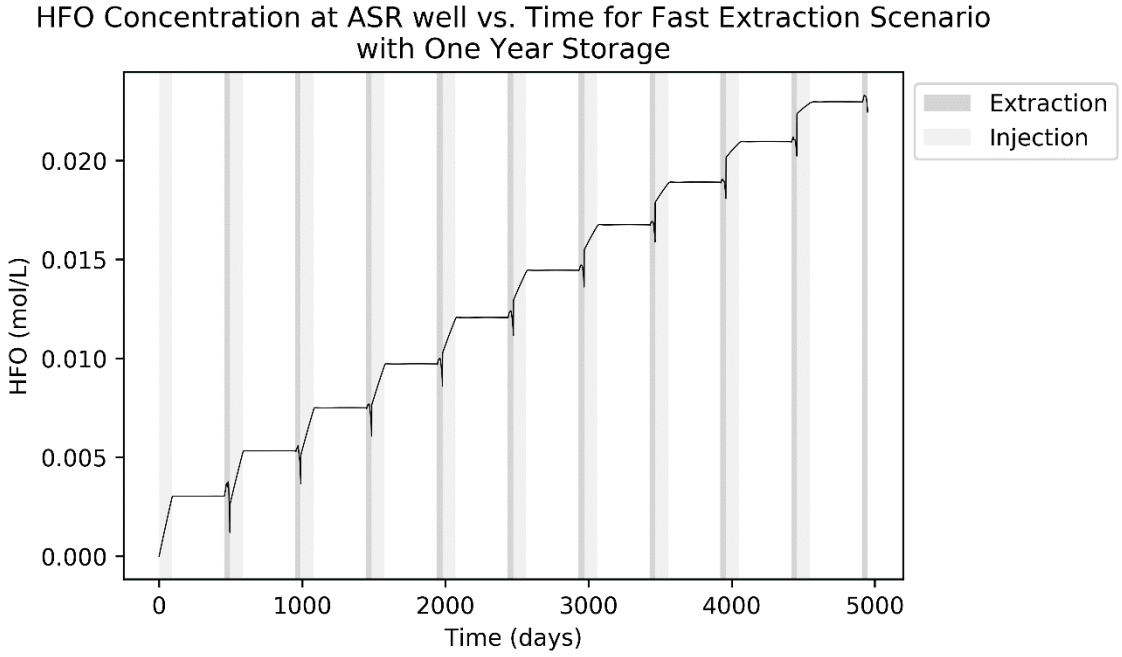
HFO Concentration at ASR well vs. Time for Fast Extraction Scenario
with One Year Storage
HFO (mol/L)
0.000
0.005
0.010
0.015
0.020
0
1000
2000
3000
4000
5000
Time (days)
Extraction
Injection

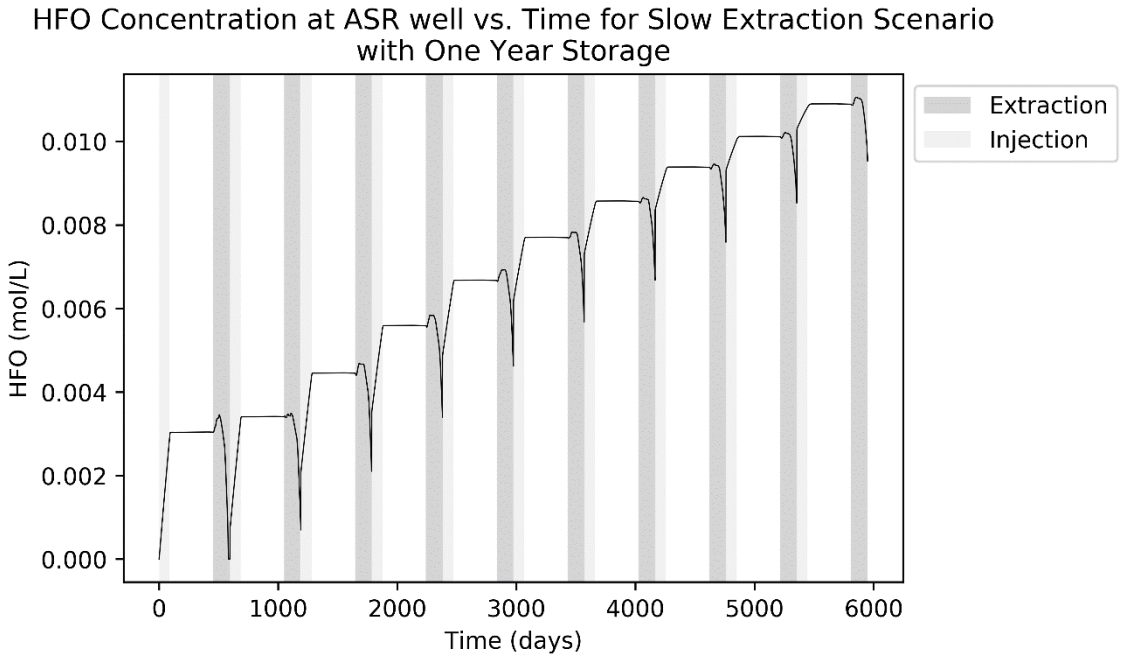
HFO Concentration at ASR well vs. Time for Slow Extraction Scenario
with One Year Storage
Extraction
Injection
HFO (mol/L)
0.000
0.002
0.004
0.006
0.008
0.010
0
1000
2000
3000
4000
5000
6000
Time (days)